

A Publication Of Indian Society For Radlation And Photochemical Sciences

SEPTEMBER, 2008

Vol.20, Nos. 2 & 3

ISRAPS

Bulletin



Guest Editor
Samita Basu



Volume 20, Number 2&3

ISRAPS Bulletin

A Publication of
Indian Society for Radiation and Photochemical Sciences

September, 2008

Editorial

It is a privilege on my behalf to present the following articles for this current issue of ISRAPS Bulletin. It is noteworthy that this issue cites six articles of varied interest in the field of photochemistry. The first article written by Dr. R. Swaminathan describes recent developments in the field where fluorescence can be employed to monitor dynamic events in real time inside living cells and animals. Dr. Mintu Halder has introduced a new method for the determination of critical micellar concentration based on the calculation of reorganization energy of a solvent sensitive fluorescent probe located at the micellar aggregate. Photoluminescent semiconductor nanoparticles or quantum dots have interesting optoelectronic properties with real and potential applications in science and technology. Dr. Debabrata Mandal has described in his article the synthesis as well as steady-state and time-resolved spectroscopy of such photoluminescent CdS and CdS:Mn²⁺ nanoparticles. Again Dr. Sivaprasad Mitra has cited steady-state and time-resolved studies on some photoinduced intramolecular processes in homogeneous and cyclodextrin nanocavities. Dr. Nitin Chattopadhyay and his coworkers have attempted to justify the name of fluorescence resonance energy transfer as a true 'spectroscopic ruler' by citing a few examples of photoreactions in different environments and illustrating its wide applicability in the determination of distances between the two partners involved in the process. The final article by Dr. Ranjan Das tells about the use of time-resolved electron paramagnetic resonance spectroscopy to provide experimental evidence of the involvement of triplet excited state in the photodissociation of hydrogen peroxide. I gratefully acknowledge the valuable contributions of the authors, because, without their help and cooperation it would not have been possible to publish this issue.

(Samita Basu)



Dr. Samita Basu did her Graduation and Masters from Calcutta University. She worked with Prof. Mihir Chowdhury at Indian Association for the Cultivation of Science, Jadavpur, Kolkata and obtained her PhD degree in 1989 from Jadavpur University, Kolkata. At present she is Professor in the Chemical Sciences Division, Saha Institute of Nuclear Physics, Kolkata. Her research interests include studies of photoinduced electron transfer reactions, drug-DNA and drug-protein interactions, etc. using steady-state and time-resolved absorption and fluorescence spectroscopy with associated magnetic field effects.

ISRAPS EXECUTIVE COUNCIL 2008-2010

President:

Dr. Tulsi Mukherjee

Vice-Presidents:

Dr. Sisir K. Sarkar

Dr P.N. Bajaj

Secretary:

Dr. Tapan K. Ghanty

Treasurer:

Dr. S. Dhanya

EXECUTIVE MEMBERS

Prof. Samita Basu

Dr. D.B. Naik

Dr. Haridas Pal

Prof. K. Pitchumani

Dr. B.S.M.Rao

Prof. Anunay Samanta

Dr. R.K. Vatsa

CO-OPTED MEMBERS

C.T. Aravindkumar

Dr. T. Bandyopadhyay

Dr. H.N. Ghosh

Dr. Sanjay Pant

Dr. C.N. Patra

Prof. P. Ramamurty

Dr. Sunil Sabharwal

Dr. A.V. Sapre

Prof. A. K. Singh

Dr. H. P. Upadhyaya

Message from the President and Secretary

Dear Members of ISRAPS and Readers,

Greetings from the new Executive Council of ISRAPS! The year 2008 started with holding the Trombay Symposium on Radiation & Photochemistry (TSRP 2008) being organized outside Mumbai for the first time at YASHADA, Pune, during January 7 - 11, 2008, which was sponsored by the Board of Research in Nuclear Sciences in collaboration with ISRAPS. Just before TSRP-2008, a Workshop on Radiation and Photochemistry was organised at Bhabha Atomic Research Centre, Mumbai, during January 3-5, 2008. Election of Executive Council was held last year and the results have been announced in the AGBM of ISRAPS held during TSRP-2008.

All our efforts in recent months have been focussed on the preparation for organising National Symposium on Radiation & Photochemistry to be held during March 12-14, 2009 at Kumaun University, Nainital. Preparation for holding an ISRAPS Discussion Meeting on "Advanced Techniques in Radiation and Photochemistry" is also underway.

Finally, we would like to thank Prof. Samita Basu, the Guest Editor of this special issue, for her efforts in bringing out a scientifically rich issue of ISRAPS bulletin containing six articles of varied interest in the field of photochemistry. Thanks are also due to all the authors for contributing articles.

We wish to express our gratitude to each and every member of ISRAPS for their ample support and cooperation in carrying out the activities of the society.



(Dr. Tulsi Mukherjee)
President



(Dr. Tapan K. Ghanty)
Secretary

Tracking dynamic events in biology using fluorescence: From macromolecules in test tube to cells deep inside living animals

R. Swaminathan

Department of Biotechnology, Indian Institute of Technology Guwahati,
Guwahati 78103, Assam, India.
e-mail: rsw@iitg.ernet.in

This article describes how fluorescence can be employed to monitor dynamic events in real time inside living cells and animals. Recent developments in the field are highlighted.

Observing the dynamic events in molecular detail in a protein for example, or inside a living cell or inside the organ of a living animal both non-invasively and in real time has been an important challenge in biology for a long while. Such events may include but not limited to protein conformational changes, protein-ligand binding, protein-DNA interactions, enzyme-substrate encounter, protein-protein interactions, movement of cells like red blood cells during blood flow and so on. Such a technology is today relevant for both early diagnosis and treatment of diseases. Borrowing the words of George Whitesides, "In the near future it is likely that we shall be moving from treating disease to anticipating disease".

Fortunately, rapid advances in probe design, instrumentation hardware and detection technology have enabled fluorescence based techniques to successfully meet this challenge in biology to a significant extent, although a lot remains to be done. It is indeed hard to imagine that this all began just fifty years ago when Prof. Gregorio Weber measured fluorescence from tryptophan [1]. The goal of this article is not to give an exhaustive review of relevant fluorescence applications in the

context stated above, but to touch upon some aspects including recent developments. The idea here is to stimulate young minds to take up challenging problems in biology using fluorescence as a tool.

Biology has in the past endured a reductionist view where every enzyme/protein/DNA has been looked at mostly in isolation in a purified state inside a test tube. Fortunately, advances in spectroscopy together with rapid advances in molecular biology over the past several decades bringing about the OMICS revolution (Genomics/Proteomics) has changed that view. Today biologists are no longer content to look at static three dimensional crystal structures of protein/DNA or the two dimensional slices from transmission electron microscope, they wish to include the fourth dimension, i.e. time [2]. How does the atomic coordinates of the macromolecule change with time? The answer to the above question defines dynamics [2].

A living prokaryotic (bacteria) or eukaryotic (human) cell requires a host of proteins which work like molecular machines to perform the housekeeping activities of the cell like breakdown of nutrients (metabolism), transport of wastes outside, DNA replication, transcription & translation, cell division which are essential for cell survival. The new field of 'Systems Biology' looks at all the above events together as they happen, unraveling the

chain and network of molecular players involved [3]. These inputs are necessary today to develop a better understanding of the cellular dynamics.

WE now return to our original challenge, namely how to monitor dynamic events in a living cell or organ. Here fluorescence offers several advantages, chief among them is the fact that it is NON-INVASIVE. Contrast this with a technique like transmission electron microscopy which can offer spatial resolutions on the atomic scale, but cannot be employed to study living specimens owing to the harsh sample preparation techniques including nanometer level thickness of the sample.

In order to study events related to a specific protein inside a cell, labeling the protein with a fluorescent probe is essential because intrinsic fluorescence from cell components is weak and non-specific [14]. Currently there are no easy solutions to this problem. Several approaches have been tried, like microinjecting the probe/probe conjugated protein inside the cell [4], employing membrane permeant derivatives of probe, using fluorescently tagged antibody specifically targeted towards the desired protein and so on [5]. A big drawback of these techniques is that they all significantly perturb the normal cell. In the early 1990's the discovery of green fluorescent protein from the jellyfish *Aequorea victoria* revolutionized biology and solved this problem to a significant extent [6]. GFP or its variants can be expressed as a fusion protein with the desired protein of interest endogenously, thereby circumventing the problems associated with introducing the probe inside the cell above [7]. But GFP is not the best solution for all occasions because of its ~30 kDa size which can be an issue at times. Several improvements like FiAsH have since arrived [5].

Once a protein is fluorescently labeled, there are a number of well established techniques [8] like fluorescence resonance energy transfer, fluorescence recovery after photobleaching [9], fluorescence correlation spectroscopy, fluorescence anisotropy and so on which can be employed to look at the dynamics of the protein inside the cell employing a fluorescence microscope [10]. But how does one observe dynamic events within cells that are present in hollow tissue tracts or deep inside the organ of the living animal at high resolution? This is equivalent to taking a miniaturized fluorescence microscope inside the ear or brain and looking at the fluorescently labelled cells inside. Recent advances in fiber-optic fluorescence imaging have made it possible to image non-invasively deep inside tissues in living animals [11]. Mark Schnitzer and coworkers have built a portable multiphoton fluorescence microendoscope with an imaging head that weighs 3.9 grams using compound gradient refractive index (GRIN) lenses and a flexible photonic bandgap fiber that enables transmission of ultrashort excitation pulses with minimal distortion [12]. They have employed this microendoscope to image blood vessels labeled with fluorescein in the brain of live mice at micrometer resolution [12]. In another work it has been shown that blood flow velocities in the cochlea of live guinea pigs can be measured using one photon fluorescence microendoscopy in an epifluorescence configuration employing intravenously injected fluorescein as the dye [13]. They observed passage of individual red blood cells as a single file through the individual capillaries with blood flow velocities reaching upto 500 $\mu\text{m}/\text{s}$ [13].

The above examples underscore the fact that demands of basic research in medicine, health care and biology are today

propelling the fluorescence technologies to new heights. More and bigger advances are likely in the future.

References

1. F. W. J. Teale and G. Weber, Ultraviolet fluorescence of the aromatic amino acids, *Biochem. J.* 65, 476-482 (1957).
2. K. Henzler-Wildman and D. Kern, Dynamic personalities of proteins, *Nature*, 450, 964-972 (2007).
3. Y. Lazebnik, Can a biologist fix a radio? -Or, what I learned while studying apoptosis, *Cancer Cell* 2, 179-82 (2002); Kitano H., Systems biology: a brief overview., *Science*, 295, 1662-1664, (2002); M.E. Csete and J.C. Doyle, Reverse engineering of biological complexity, *Science*, 295, 1664-1669 (2002)
4. Live Cell Imaging: A laboratory manual by R. D. Goldman and D. L. Spector, Cold Spring Harbor Laboratory Press, New York, 2005.
5. Ben N. G. Giepmans, Stephen R. Adams, Mark H. Ellisman, Roger Y. Tsien, The Fluorescent Toolbox for Assessing Protein Location and Function, *Science*, 312, 217-224 (2006)
6. R. Y. Tsien, The green fluorescent protein, *Annu. Rev. Biochem.*, 67, 509-544 (1998).
7. J. Lippincott-Shwartz and G. Patterson, Development and Use of Fluorescent Protein Markers in Living Cells, *Science*, 300, 87-91 (2003).
8. Principles of Fluorescence Spectroscopy by J. R. Lakowicz, 3rd Ed., Springer, Singapore, 2006.
9. J. Lippincott-Shwartz, N. Altan-Bonnet and G. Patterson, Photobleaching and photoactivation: following protein dynamics in living cells, *Nature Cell Biol.*, 5, S7-S14 (2003).
10. David J. Stephens and Victoria J. Allan, Light Microscopy Techniques for Live Cell Imaging, *Science*, 300, 82-86 (2003).
11. B. A Flusberg, E. D Cocker, W. Piyawattanametha, J. C Jung, E. L M Cheung and M. J Schnitzer, Fiber-optic fluorescence imaging, *Nature Methods*, 2, 941-950 (2005).
12. B. A. Flusberg, J. C. Jung, E. D. Cocker, E. P. Anderson, and M. J. Schnitzer, *In vivo* brain imaging using a portable 3.9 gram two-photon fluorescence microendoscope, *Optics Letters*, 30, 2272-2274, (2005).
13. Ashkan Monfared, Nikolas H. Blevins, Eunice L. M. Cheung, Juergen C. Jung, Gerald Popelka and Mark J. Schnitzer, *In Vivo* Imaging of Mammalian Cochlear Blood Flow Using Fluorescence Microendoscopy, *Otology and Neurology*, 27, 144-152 (2006).
14. A. Miyawaki, A. Sawano and T. Kogure, Lighting up cells: labeling proteins with fluorophores, *Nature Cell Biol.*, 5, S1-S7 (2003).



Dr. Rajaram Swaminathan is presently affiliated as Associate Professor, Department of Biotechnology, Indian Institute of Technology Guwahati, Guwahati 781 039, Assam, INDIA. He obtained his Master of Science in Biotechnology in 1990 from the Indian Institute of Technology, Bombay, and then his Ph.D. degree in 1996 from the Tata Institute of Fundamental Research, Mumbai. For the period of 1995-98 he did his post-doctoral research in the University of California, San Francisco, USA. For the period of 1998-99 he worked at the National Centre for Ultrafast Processes, Chennai as a Project Associate. Dr. Swaminathan joined the Indian Institute of Technology, Guwahati as a Faculty in the year 1999. His current interest includes (1) Molecular events in Protein Aggregation, (2) Influence of Macromolecular Crowding on enzymatic reaction rates & equilibria, and (3) Applications Fluorescence Spectroscopy in diagnostics. He is having an impressive number of research publications in national and international journals.

Application of reorganization energy calculation in the determination of critical micellar concentration of a micelle

Priyanka Bolel and Mintu Halder*

Department of Chemistry, Indian Institute of Technology Kharagpur, Kharagpur-721 302

*E-mail: mintu@chem.iitkgp.ernet.in

Abstract

This is a new method for the determination of critical micellar concentration (CMC) based on the calculation of reorganization energy of a solvent sensitive fluorescent probe located at the micellar aggregate. The variation of reorganization energy with respect to bulk water is a result of the formation of micelles from the surfactant monomer, here, cetyl trimethyl ammonium bromide (CTAB) and is calculated from the ref 10 using emission and excitation spectra of the probe. Earlier methods reported in literature were based on surface tension measurement, micellar catalysis and many other methods. The reorganization energy results from the creation of a transient solute dipole (by an exciting photon) in a solvent atmosphere. This induces a reorganization of the solvent molecules (dipoles; for non-polar solvents - no reorganization) about the dipole in a manner that stabilizes the energy of the system, and the energy term thus involved is referred to as the reorganization energy.

Introduction

Surfactants are surface active molecules containing a hydrophobic long-chain (tail) as well as a polar head group. These molecules spontaneously form stable aggregates when dissolved in polar solvents like water. Such aggregates are called normal micelles (see Figure 1) [1,2]. There is a particular concentration (the critical concentration), characteristic of the surfactant (in a given

solvent) at or above which these surfactants will form micelles, which is called the critical micellar concentration (CMC).

Before the critical concentration is attained aggregates may still be formed, which are pre-micellar aggregates [3]. The micellar aggregates contain a certain number of monomer units on the average, which is called as aggregation number.

The formation of micelle from surfactant monomer with aggregation number n could be represented by the following scheme:



This equilibrium is mostly shifted to right hand side. Micelles are highly dynamic aggregates and rates of uptake of monomers into micellar aggregates are nearly in the diffusion-controlled limit [4, 5]. Initially, when the concentration is very low these monomers behave like independent molecular entities in the solvent. As the concentration is increased they tend to come close to each other and form aggregates of various sizes as the process of aggregation is favored thermodynamically. In the vicinity of the CMC a sharp change in some observables are noticed and based on that fact the formation of micelles can be followed by several methods. There are many methods available in literature for the determination of the CMC [6, 7]: surface tension, spectrophotometric, kinetics, conductivity, osmotic pressure, fluorescence spectroscopy [8] etc.

It has already been reported by one of the present authors that CMC can be determined by monitoring Stokes shift as a function of monomer concentration [9]. Stokes shift is defined as the difference of emission and excitation maxima expressed in energy (wave number) scale. It gradually moves to the higher value with monomer concentration until CMC is reached and remains practically constant with further increase in monomer concentration beyond CMC. This variation of Stokes shift can be correlated with the environment (polarity) sensitivity of the molecular probe used as marker in the experiment. Probe molecules exhibit this polarity (environment) sensitivity because of considerable difference in its dipole moment at the ground and excited electronic states. This phenomenon of polarity sensitivity can also be looked in terms of reorganization energy of the solvent environment. Due to photonic excitation probe molecule exists as a highly polar transient solute in the excited electronic state which induces the reorganization of solvent molecules about itself in such a manner that stabilize the energy of the probe-solvent system. The energy term thus involved is called reorganization energy (λ). So, the value of reorganization energy depends upon the ability of immediate surrounding molecules to stabilize the transient polar entity through reorganization. It is important to note that solvent polarity has got a special role to play on the magnitude of reorganization energy likewise Stokes shift. Reorganization energy and Stokes shift are related by the following relation, [10].

$$\text{Reorganization energy } (\lambda) = \frac{1}{2} [\text{Stokes Shift}]$$

Let us look into the process of formation of micelles right from the monomer state in the presence of probe molecules. It is evident that these probe molecules experience a gradual change in local polarity as we

moved from bulk water (more polar, no surfactant added) to organized surfactant assembly (less polar, at and beyond CMC) with increase in monomer concentration provided the probe molecules get bound to the aggregates. This brings in a variation of λ value with monomer concentration, and in the vicinity of the CMC there is an inflection. Reorganization energy should follow the similar trend as Stokes shift and hence, calculation of reorganization energy of such system would entail us in determination of CMC of a micelle.

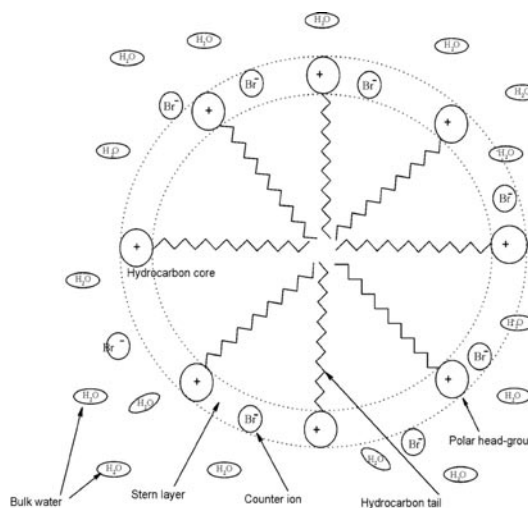


Fig. 1: Micellar aggregate (An aqueous CTAB micelle).

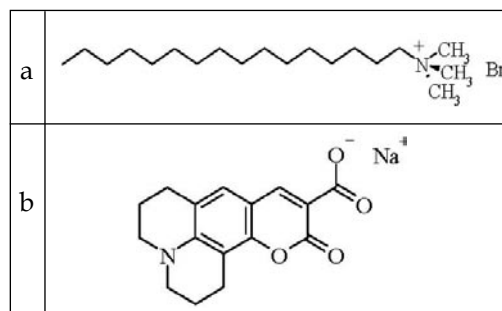


Fig. 2: Stick diagram for (a) CTAB, (b) C-343 Na Salt.

In the present experiment hexadecyltrimethyl ammonium bromide (cetyl trimethyl ammonium bromide, CTAB; a positively charged surfactant) (See Figure 2a) is used and a negatively charged polar molecule, sodium salt of coumarin-343 (see Figure 2b), is used as an environment sensitive probe.

In the present case, the micellar aggregates so formed in water are positively charged. Naturally, a negatively charged probe is likely to bind to this positively charged micelle and micellar interface will be the preferred location of the negatively charged probe because of the positive zeta-potential and the probe is not expected to prefer the non-polar hydrocarbon interior. Thus, the electrostatic force of attraction will bind the probe with the aggregate [9]. The success of this experiment depends on two important factors: (i) the stabilization of electronic states of probe molecule and (ii) probe should preferentially attach to the aggregate.

Materials and Methods

Coumarin-343 (C-343) was purchased from Exciton and CTAB from Aldrich and those were used as received. The salt of the dye was made by neutralizing it with aqueous NaOH. The concentration of the dye was maintained at $\sim 1 \times 10^{-6}$ M in the final mixture. Sets of solutions were made with varying concentrations of CTAB and a fixed concentration of the dye. The CTAB concentration in the solutions was varied up to 1.5 mM with an increment of 0.1 mM. For this, a varying amount of 10 mM CTAB solution was mixed with a varying amount of water to reach the required concentration of CTAB, keeping the total volume of mixture fixed, and to all prepared solutions a fixed small amount (1 μ L, this volume does not bring about any

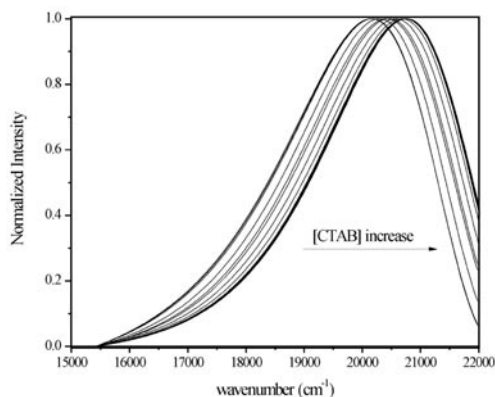


Fig. 3: Normalized emission spectral line shape of C-343 Na salt with varying concentrations of CTAB in water.

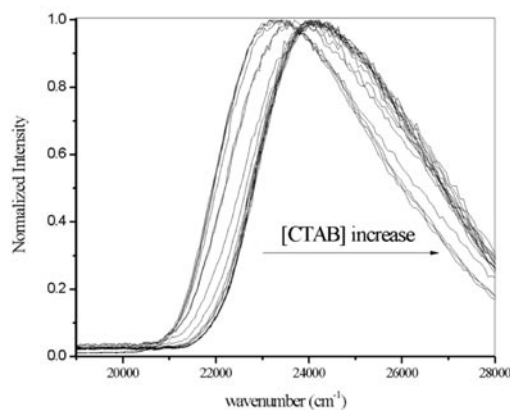


Fig. 4: Normalized excitation spectral line shape of C-343 Na salt with varying concentration of CTAB in water.

change of CTAB concentration practically) of the stock dye solution was added to reach the target dye concentration in the final mixture. All solutions were prepared with deionized or distilled water and then allowed to equilibrate for 15 to 20 minutes. Emission spectra were recorded at 440 nm and excitation spectra were monitored at 620 nm using a 1-cm-path-length cuvette and a Perkin Elmer MPF 44B spectrofluorimeter. The emission and

excitation spectra were converted to spectral line shape by appropriate mathematical transformation.

Calculation of Reorganization Energy (λ)

Reorganization energy (λ) is one of the most important parameters associated with the salvation dynamics experiment, which is widely used as a measure of the strength of interactions between a chromophore and its surrounding dielectric media. Traditionally λ value is taken as half of the Stokes shift which is the difference in peak maxima of the corresponding absorption and emission spectra.

$$\lambda = \frac{1}{2} \hbar [\max \{\sigma_a(\nu)\} - \max \{\sigma_f(\nu)\}] \quad (1)$$

Where $\max \{\sigma_{a,f}(\nu)\}$ is the maximum of the absorption (or excitation) and emission spectra respectively, on a wave number scale. However equation (1) is valid if the absorption and emission spectra are Gaussian. For most of the fluorophores however this is not the case, that is, spectra deviates significantly from Gaussian shape. Consequently eq (1) is not valid. Song and coworkers [10] have developed a methodology for the calculation of λ which implicitly takes care of the actual shape of the corresponding spectra according to the following equation.

$$\lambda = \hbar \frac{\int_0^{\infty} d\nu [\sigma_a'(\nu) - \sigma_f'(\nu)] \nu}{\int_0^{\infty} d\nu [\sigma_a'(\nu) + \sigma_f'(\nu)]} \quad (2)$$

Where $\sigma'_{a,f}$ are the absorption (or excitation) and emission spectral line shapes, respectively.

The methodology for the calculation of λ from the experimental absorption (or excitation) and emission spectra is given below.

1) Experimentally observed normalized excitation (or absorption) and emission spectra are manipulated so that couple of data points at the extreme red edge of the emission spectrum is set equal to zero. Generally, this is accomplished by subtracting the intensity value at the extreme red edge from the whole spectrum and then normalizing it to unity again. This manipulation is required because in some cases the emission spectrum does not go to zero even at the tail end due to contribution from the correction factor file of the instrument.

2) These spectra are converted to the corresponding spectral line shape according to equation (3) and (4) and normalizing to unity.

$$\sigma'_a(\nu) = \{\sigma_a(\nu)\} / \nu \quad (3)$$

$$\sigma'_f(\nu) = \{\sigma_f(\nu)\} / \nu^3 \quad (4)$$

Where $\sigma'_{a,f}$ are the absorption (or excitation) and emission spectral line shapes, respectively.

3) The excitation (or absorption) and emission spectral line shapes are manipulated so as to permit their addition and subtraction. This procedure required an interpolation of the corresponding spectral line shapes into equally spaced data points. Typically a spacing of 20-25 cm^{-1} between consecutive data points is used in each curve.

4) The curve crossing point (crossing of the excitation and emission curves) is carefully estimated by eye inspection. For this it might be required to zoom in the curve-crossing region. This curve crossing frequency gives the frequency of 0-0 transition for the system considered. This characteristic frequency has to be subtracted from the

wave number scales, so that the curve crossing point appears at zero in the abscissa.

- 5) An appropriate number of zero are added to the high energy end of the emission spectrum and the low energy end of the excitation (or absorption) spectrum so as to allow the addition and subtraction in the entire spectral region. At this point it is always better to check the maximum intensities in the corresponding spectra and if necessary, they should be renormalized to unity.
- 6) Value of λ can now be calculated using the equation (2). Typically instead of integrating from zero to infinity the integration of numerator and denominator of equation (2) is done from negative infinity to zero to avoid any contamination from higher excited states (upper states) in the excitation (or absorption) spectrum.

Results and Discussion

Emission spectral line shape for the C-343-Na salt in a CTAB/water system has been shown in Figure 3. The maxima are shifted to the higher frequency near the CMC with increasing surfactant concentration. There is no significant shift in emission maxima when the surfactant concentrations are much below or above the CMC. Similar effects are observed in the excitation spectra (Figure 4): the maxima are shifted to the higher-energy side. This means that possibly the ground state of the probe is also destabilized energetically as a result of its incorporation into less polar aggregates. Water, being a highly polar hydrogen-bonding solvent, could bring about significant stabilization of the electronic state of the polar probe as opposed to the less polar environment inside the aggregate.

It has been observed that the shift in excitation maxima is more than that of emission, which results in a net increase in the reorganization energy. Reorganization energy gives an estimate about energy requirement for reorganization of surrounding solvent molecules around a polar solute (transient) for stabilizing the system or this may be looked upon as the energy requirement to disorganize the surrounding solvent molecules about polar entity from an initially organized state. Analysis of fig.5 shows the gradual increase of reorganization energy with surfactant concentration until a certain concentration is reached, and remains practically constant with further increase of monomer concentration. The point of inflection corresponds to the CMC value. Before CMC is reached the observed increasing trend of λ with increasing monomer concentration is consequence of the decrease in local polarity of the medium. After reaching CMC practically no further increase in λ with monomer concentration indicates that there is no further reorganization of solvent atmosphere as the process of micellization has been complete.

To determine the point of inflection and hence the CMC from Figure 5, the rising part and the plateau have been fitted with linear functions. These two fitted lines cut each other at a point corresponding to the inflection [12], which has been found to be at ~ 0.9 mM and this value is in good agreement with the literature reported value from other methods [13]. To get a good result one can fit the individual spectrum with a lognormal function [14]. The fitting function can be used in scientific graphing software, like Origin or similar software. Depending on the noise in the spectra the error in determining the reorganization energy has been found to vary up to ~ 30 cm^{-1} .

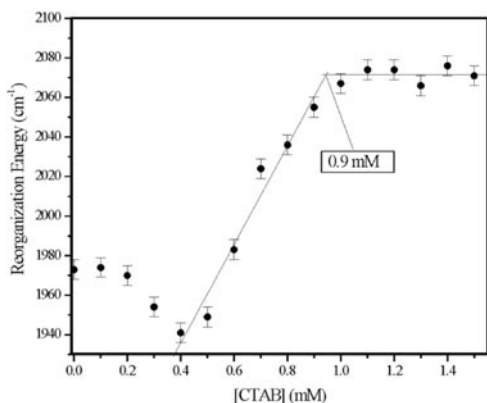


Fig. 5: Reorganization Energy of C-343 Na salt with varying concentration of CTAB in water. Vertical lines with cap indicate error bars.

Conclusion

The reorganization energy implies the energy required to reorganize the solvent molecules around a polar solute. It has been monitored as a function of monomer concentration. Beyond CMC no further change in reorganization energy indicates that no further reorganization of solvent molecules is encountered, as the micelle formation is complete. So, variation of reorganization energy with surfactant concentration is a convenient method for probing the micellization process.

Earlier CMC has been determined from the variation of Stokes shift. Stokes shift is an easily determinable quantity as it does not require intense mathematical calculation and simply by locating maxima of excitation and emission spectra this can be calculated. But this process has the disadvantage of spectral broadening. The value of Stokes shift may be erroneous if the maxima of absorption and emission spectra are broad. It becomes difficult to locate the

exact peak position due to broadness of the spectrum. The reorganization energy calculation is devoid of such disadvantage because it takes in account the shape of a whole spectral function rather than a single point and careful inspection of peak maxima is not so important here. The current method requires that the spectral shape should be close to gaussian which we can take care of with a suitable probe molecule.

Similar experiments can be carried out with other cationic surfactants, such as cetyl pyridinium chloride (CPCl) using the same C-343.Na salt as the probe. For anionic surfactants, one can, in principle, apply a similar method.

Acknowledgement

We thank DST-India, CSIR-India and IIT Kharagpur for financial assistance.

References and Notes

1. Menger, F. M. *Acc. Chem. Res.* 1979, 12, 111–117
2. Morai, Y. *Micelles*, Plenum Press, NY, 1982.
3. Kunitake, T. *Angew. Chem., Int. Ed. Engl.* 1992, 31, 709–726.
4. Sams, P. J.; Wyn-Jones, E.; Rassing, J. *Chem. Phys. Lett.* 1972, 13, 233–236.
5. Aniansson, E. A. G.; Wall, S. N.; Almgren, M.; Hoffmann, H.; Kielmann, I.; Ulbricht, W.; Zana, R.; Lang, J.; Tondre, C. *J. Phys. Chem.* 1976, 80, 905–922.
6. Hunter, R. J. *Fundamentals of Colloid Science*, Vol. 1&2; Oxford University Press: New York, 1989.
7. Atkins, P. W. *Physical Chemistry*; W. H. Freeman and Co.: New York, 1998.
8. Kalyanasundaram, K. *Photochemistry in Microheterogeneous Systems*; Academic Press, New York, 1987.
9. Halder, M., *The Chemical Educator* 2007, 12, 33–36.

10. Jordanides, X. J., Lang, M. J., Song, X. and Fleming, G. R., *J. Phys.Chem. B* 1999, 103, 7995-8005.
11. Haldar, M.; Chowdhury, M., *Chem. Phys. Letts.* 1999, 312, 432-439.
12. Dominguez, A.; Fernández, A.; Gonzalez, N.; Iglesias, E.; Montenegro, L., *J. Chem. Educ.* 1997, 74, 1227-1231.
13. Huang, X.; Yang, J.; Zhang, W.; Zhang, Z.; An, Z. *J. Chem. Educ.* 1999, 76, 93-94.
14. Maroncelli, M.; Fleming, G. R. *J. Chem. Phys.* 1987, 86, 6221-6239
15. Jordanides, X. J.; Lang, M. J.; Song, X.; Fleming, G. R. *J. Chem. Phys.* 1999, 110, 5884-5892.



Dr. Mintu Halder was born in Kolkata. He got his B. Sc. and M. Sc. degrees from the University of Calcutta. He did Ph. D. with Prof. Mihir Chowdhury, from the Indian Association for the Cultivation of Science, Jadavpur in 2000. Then he moved to Iowa State University, USA, for his post doctoral research, where he worked on Biophysics and Ultrafast Spectroscopy. Currently Dr. Halder is in the Department of Chemistry, IIT Kharagpur. His research interests include Biophysics, Photophysics and related aspects, Chemical education and Instrumentation.



Priyanka Bolel did her B.Sc with Chemistry Honours from Hooghly Mohsin College, Chinsurah under University of Burdwan in the year 2004. She completed her M. Sc. with Physical Chemistry as specialization from the department of chemistry of the same University in 2006. At present she is pursuing Ph. D. research in spectroscopy of chemical and biochemical systems at IIT Kharagpur Chemistry under the guidance of Dr. Mintu Halder.

Synthesis and spectroscopy of photoluminescent CdS and CdS:Mn⁺² nanoparticles

Debabrata Mandal

Department of Chemistry,

Visva-Bharati University, Santiniketan 731 235, India

E-Mail: mandaldeb@yahoo.com

Introduction

Photoluminescent semiconductor nanoparticles or quantum dots have interesting optoelectronic properties with real and potential applications in science and technology. The two key structural parameters that determine these properties are the size of the particles and their surface characteristics [1-3]. In a semiconductor crystal of nm-scale size, the absorption band-gap is a function of the particle size. This is known as the quantum confinement effect, which becomes important when the particle dimensions become comparable to the Bohr radius of the hole-electron exciton [1]. Thus the absorption spectra and related properties (e.g., color) of a semiconductor material can be tuned over a considerably wide range by simply varying the size of the nanoparticles [1]. On the other hand, due to the extreme small size of the nanoparticles (typically $\leq 5\text{nm}$), the surface-volume ratio is quite high. For example, a 5 nm diameter CdS particle has almost $\sim 15\%$ atoms at the surface [3]. Naturally, the surface characteristics have an important role in determining several important nanoparticle properties, most notably the photoluminescence.

The photoluminescence (PL) of II-VI semiconductor nanoparticles is attributed to the decay of photo-generated charge carriers by radiative recombination. Two major types of PL are identified. One is the high-energy emission near the long wavelength

edge of the band-gap absorption, caused by electron-hole pair (exciton) recombination at the band edge. The other is a broad emission over a range of energies lower than the band-gap, caused by recombination at "trap" states mainly localized near the surface and having energy levels in the forbidden band gap [1-2]. Surface treatment with a suitable material can lead to passivation, i.e., suppression of the surface defects which act as trap states, thus improving both the photostability and quantum efficiency [4-5]. Further, nanoparticles can be attached to a host macromolecular or supramolecular body through covalent or coordinate bond formation at the surface states, vastly improving their versatility. According to several recent reports, owing to their high photostability and versatility, photoluminescent semiconductor nanoparticles are poised to replace organic fluorescent molecules for important biological tagging/ imaging applications [6-7].

From a chemists' point of view, another noticeable advantage of semiconductor nanoparticles is the availability of numerous wet-chemical methods for their synthesis. These afford a rather simple means to control nanoparticle structural parameters by manipulating synthetic conditions like nature of solvent, temperature, stabilizing agent, rates of addition of different reagents, etc [1-3, 6-7]. A nanoparticle solution prepared by

wet-chemical methods essentially consists of insoluble particles in the size range ≤ 5 nm, dispersed in a liquid medium and protected from coagulation and precipitation by ionic or steric stabilization. Some of the most widely used stabilizing agents are polymers including chain polymers [8] and oligomers [9], dendrimers [6-7] and block copolymers [10]. Polymers provide not only efficient steric stabilization but also facilitate subsequent processing steps like film casting which are crucial in large-scale device fabrication.

In this paper, we will describe the synthesis of CdS and CdS:Mn⁺² (i.e., Mn⁺²-doped CdS) nanoparticles following a simple solution-phase reaction between readily available ionic precursors in alcohol solvents, with the well-known polymer, Polyvinylpyrrolidone (PVP), as stabilizer. Steady-state and time-resolved spectroscopy were also performed on the synthesized nanoparticles, which reveal their band-gap transition and PL characteristics. Further, the effect of Mn⁺² doping on the PL was also investigated

Experimental

CdS nanoparticles were prepared in 4 different alcohols: methanol, ethanol, 1-propanol and 1-hexanol, with PVP as a polymeric stabilizer. To 10 mL of any of the alcohols in a round-bottomed flask was added 20 μ L of 0.12 M of aqueous solution of Cd(NO₃)₂·4H₂O and 50 μ L of 10% (w/v) methanolic solution of PVP. After stirring for 30 min., 20 μ L of 0.2 M of aqueous solution of Na₂S·9H₂O was slowly added. A greenish-yellow colour develops which intensifies with stirring, indicating the formation of UV-visible absorbing CdS semiconductor nanocrystals. The solution was left to stir overnight at room temperature. The nominal final concentration of the ions were [Cd⁺²]

= 2.4 X 10⁻⁴ M and [S⁻²] = 4.0 X 10⁻⁴ M. The polymer concentration was 0.05%. Synthesis of CdS:Mn⁺² nanoparticles was performed in 0.05% PVP/ methanol solution using a similar method as above. However, in this case, along with 20 μ L of 0.12 M of aqueous solution of Cd(NO₃)₂·4H₂O, 2 μ L of 0.012 M of aqueous solution of MnSO₄·H₂O was also added at the beginning, maintaining the nominal [Cd⁺²] : [Mn⁺²] ratio at 100 : 1.

The solutions were studied by steady state UV-visible absorption and PL spectroscopy and the changes in spectral pattern were monitored over time. At the initial stages, minor changes in the absorption / PL spectra were observed, which eventually ceased after a few days. Thereafter the solutions continued to remain stable over several weeks. Picosecond PL dynamics experiments were carried out on the stable solutions with a time-correlated single photon counting (TCSPC) setup employing a picosecond diode laser (IBH NanoLED-07) operating at a λ_{ex} = 373 nm and a repetition rate of 0.9 MHz as excitation source.

Results and Discussion

The absorption spectra of CdS in PVP/alcohol solutions, shown in fig. 1, display a clear absorption onset, with a peak around 370 - 390 nm, corresponding to the most probable hole-electron excitonic transition. The semiconductor band-gap was obtained in each case by locating the point of intersection of a tangent drawn to the sharply ascending part of the absorption spectra, with the wavelength axis. The results listed in table 1 show that the band-gap lies between 2.8 - 2.9 eV, which is >0.3 eV blue-shifted in comparison to the bulk semiconductor band-gap, i.e., 2.5 eV [2], clear evidence of strong quantum confinement in the nanoparticles. Henglein et al. have

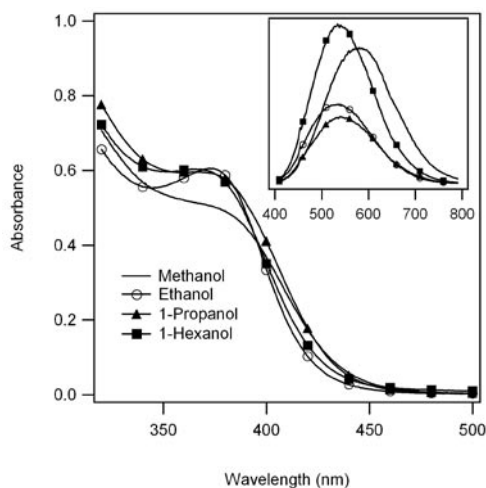


Fig. 1. Absorption spectra of CdS nanoparticles synthesized and stabilized in 0.05% PVP solutions in different alcohols. Inset shows the O.D. corrected steady state PL spectra of the solutions.

provided an empirical formula to calculate the average diameter of the particles from their band-gap wavelength λ_{bg} [11]:

$$2r(\text{nm}) = \frac{0.1}{0.1338 - 0.0002345\lambda_{bg}} \quad (\text{i})$$

The particle size calculated in this method and listed in table 1, are found to be ~ 3 nm.

The inset of figure 1 displays the steady state PL spectra of the CdS nanoparticles in PVP/alcohol solutions, with $\lambda_{ex} = 373$ nm. The spectra in each case is broad and considerably red-shifted from the main excitonic absorption peaks around 370 – 390 nm. Thus, it is obvious that the main contribution to the PL is derived from the surface-localized defects, i.e., surface trap states. The emission quantum yields of the nanoparticles were estimated to be 1-2%, calculated by taking Coumarin 153 in ethanol as standard. Although figure 1

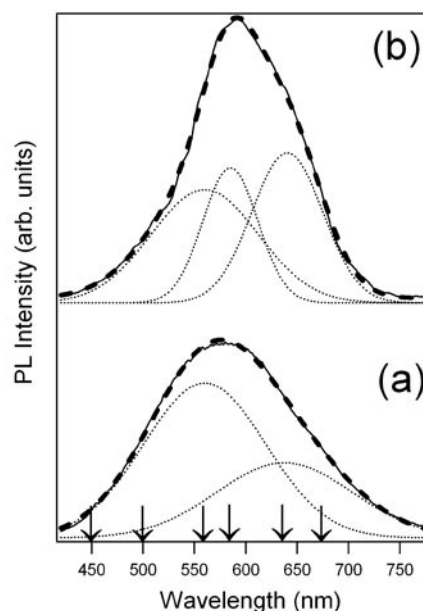


Fig. 2. PL spectra of a) CdS and b) CdS:Mn²⁺ nanoparticles, synthesized and stabilized in 0.05% PVP/methanol solution. $\lambda_{ex} = 373$ nm. The broken lines show the best fits obtained with a sum of 2 gaussian peaks (fig. 3a) and 3 gaussian peaks (fig. 3b) respectively. The dotted curves represent the individual resolved gaussian peaks, showing their positions and relative amplitudes. The arrows in a) indicate the emission wavelengths at which transient PL were recorded.

shows small variations in the absorption and PL spectra of CdS nanoparticles depending on the alcohol used, we do not observe any systematic correlation between these variations and the specific nature of the alcohol. Hence it is reasonable to assume that the spectral characteristics displayed by the nanoparticles are mainly determined by the synthetic method, nature of ionic precursors, stabilizer and temperature, rather than the nature of the alcohol solvent.

Doping the CdS nanoparticles with 1% Mn²⁺ ions leads to the formation of CdS:Mn²⁺ nanoparticles. At 1% doping, the absorption

Table 1: Spectral Characteristics of CdS Semiconductor Nanoparticles in PVP/alcohol solutions

Polymer solution	Absorption onset (nm)	Band-gap (eV)	Diameter ^a (nm)
PVP/ Methanol	440	2.82	3.25
PVP/ Ethanol	425	2.90	2.95
PVP / n-Propanol	436	2.85	3.15
PVP/ n-Hexanol	432	2.8	3.05

^a Calculated from Henglein's empirical formula (ref. 11)

Table 2: Tri-exponential fitting parameters to transient PL curves

Nanoparticle Sample	λ_{em} (nm)	a_1 (%)	a_2 (%)	a_3 (%)
CdS (undoped)	450	88	8	4
	500	82	14	4
	560	78	19	3
	585	71	25	4
	640	65	31	4
	675	59	35	6
CdS:Mn ²⁺ (1% doped)	500	54	34	11
	560	47	41	12
	585	63	26	11
	640	63	28	9

spectra remained nearly the same, but the changes in PL spectra were substantial. Figure 2 shows a comparison between the PL spectra of CdS and CdS:Mn²⁺ nanoparticles, both synthesized and stabilized in PVP/methanol. The very broad spectrum of CdS in fig. 2a, extending from 400 to 800 nm, suggests a broad distribution of trap-states with multiple emission peaks. Following a procedure reported earlier by Yang and Holloway [3], we tried to identify the major peaks by resolving the entire spectrum into a sum of several gaussians, assuming each

individual peak to have a gaussian shape. The best fit yielded two gaussians peaked at 560 nm and 640 nm, each having fwhm of ~150 nm, as shown in fig. 2a. These are strikingly similar to the peaks found by Yang and Holloway at 550 nm and 650 nm for ZnS-passivated CdS:Mn²⁺ nanoparticles, which they identified as localized trap states in the band-gap and internal defect states (probably due to S atom vacancies), respectively [3].

With 1% Mn²⁺ doping, on the other hand, the spectral shape is significantly

distorted, strongly indicating additional PL transitions. The spectrum in this case was best resolved into 3 gaussians peaked at 560 nm, 585 nm and 640 nm, as shown in fig. 2b. The additional narrower peak at 585 nm is clearly attributed to the ${}^4T_1-{}^6A_1$ transition of Mn^{+2} ions embedded in the CdS lattice [3, 11-14]. Close inspection into the relative amplitudes of the resolved peaks reveals an interesting fact. In pure CdS nanoparticles, the relative amplitudes of the 560 nm and 640 nm peaks are 67% and 33%, respectively, while in CdS: Mn^{+2} nanoparticles, the relative amplitudes of the 560 nm, 585 nm and 640 nm peaks are 29%, 38% and 33%, respectively. Thus, at 1% Mn^{+2} doping, the 560 nm loses a substantial portion of its intensity to the Mn^{+2} emission, while the 640 nm peak is left unperturbed. We interpreted the intensity loss to be a consequence of energy transfer from some of the trap states to the Mn^{+2} dopant sites, similar to the energy transfer to Mn^{+2} dopants observed in ZnS: Mn^{+2} nanoparticles [13-14]. Further support for this assignment was obtained from picosecond time-resolved PL studies.

In the time-resolved studies, the samples were excited at $\lambda_{ex} = 373$ nm and the transient PL response were recorded upto a maximum time delay of 20 ns with a time-resolution of ~ 100 ps. The PL transients for CdS nanoparticles at $\lambda_{em} = 450, 500, 560, 585, 640, 675$ nm are displayed in fig. 3a. At all λ_{em} , the early part of the decay is extremely fast, on a scale comparable to the instrument response time of ~ 100 ps. We took great care to filter out any scattered light, ensuring that this feature is indeed a transient PL and not merely due to scattering. On the other hand, the later part of the decay is too slow to be completed within the 20 ns delay time, especially at the longer λ_{em} . In other words, the PL dynamics is non-exponential, the overall rate becoming slower at longer

λ_{em} . The transients were fitted to a triple exponential decay function:

$$f(t) = a_1 \exp(-t/\tau_1) + a_2 \exp(-t/\tau_2) + a_3 \exp(-t/\tau_3) \quad (ii)$$

where the 3 time constant τ_1, τ_2 and τ_3 were in the scale of 100 ps, 1 ns and 10 ns, respectively. The fitting parameters for the best fit are listed in table 2. A systematic variation of time-constants with emission wavelength is observed, τ_1 predominating at shorter λ_{em} and τ_2, τ_3 at longer λ_{em} . It suggests that the decay rate of the trap-states decreases with decreasing emission energy, i.e., high-energy (or "shallow") traps have a shorter lifetime than low-energy (or "deep") traps, which is in agreement with previous observations in semiconductor nanoparticles [6-8, 13-14]. In general, the results confirm the heterogeneous character of the trap states primarily responsible for the CdS PL.

Figure 3b displays the PL transients of CdS: Mn^{+2} nanoparticles, collected at $\lambda_{em} = 500, 560, 585$ and 640 nm. Since here too, the decay spans several time-scales, the transients were fitted with a triple exponential decay function with the 3 time constant τ_1, τ_2 and τ_3 in the scale of 100 ps, 1 ns and 10 ns, respectively, and the best fit results are listed in table 2. From fig. 3a and 3b, it appears that the PL transients of CdS: Mn^{+2} are slower than those of undoped CdS nanoparticles at the same emission wavelength. The retardation of the overall decay rate is largely accounted for by the decreasing amplitude of the fastest, ~ 100 ps component in the doped samples. However, it is interesting to note the significant rise in the amplitude of the intermediate ~ 1 ns component in the doped samples. Earlier, Chung et al. had observed that Mn^{+2} doping of ZnS nanoparticles led to an increase in the amplitude of a ~ 700 ps component [14]. They attributed this to energy transfer

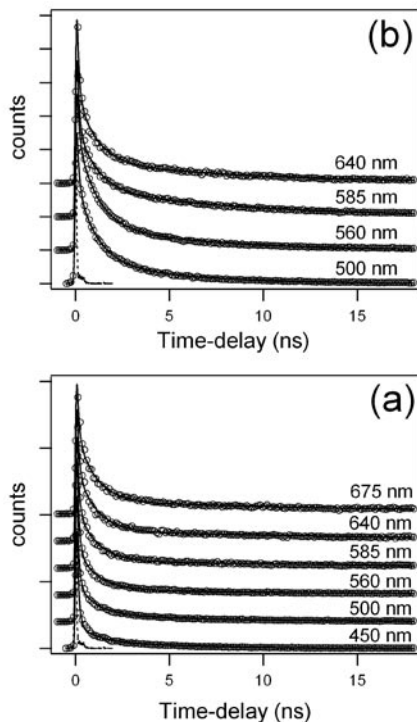


Fig. 3. Transient PL curves of a) CdS and b) CdS: Mn²⁺ nanoparticles synthesized and stabilized in 0.05% PVP/methanol solutions at different emission wavelengths, as indicated for each curve. $\lambda_{ex} = 373$ nm. The curves are displaced vertically for better visualization. The instrument response (dotted curve) is drawn for comparison.

from the trap-states to the Mn²⁺ atoms. In our system, a sizeable fraction of trap states have an intrinsic lifetime of ~ 1 ns even in the undoped CdS nanoparticles. Thus, if an energy transfer to Mn²⁺ atoms actually takes place in a 700 ps time-scale, it will effectively enhance the overall amplitude of the ~ 1 ns component, because, given the pronounced heterogeneity in the CdS trap-state dynamics, it is difficult to distinguish between a ~ 700 ps and a ~ 1 ns response.

Our results thus demonstrate that the transient PL of CdS nanoparticles are

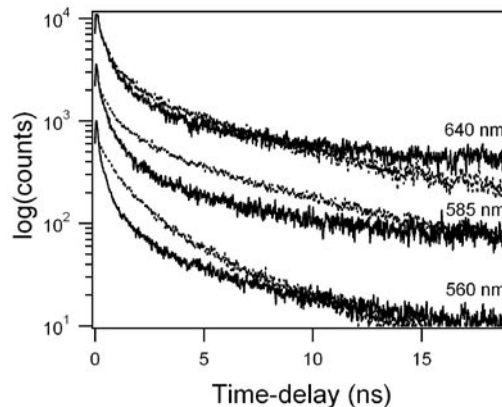


Fig. 4. Transient PL curves of CdS (solid lines) and CdS:Mn²⁺ nanoparticles (dotted lines) synthesized and stabilized in 0.05% PVP/methanol solutions at $\lambda_{em} = 560, 585$ and 640 nm, as indicated, plotted against a logarithmic y-axis for better visual comparison.

modified in presence of Mn²⁺ at even 1% doping level. At this point it is reasonable to probe whether the Mn²⁺ ions themselves contribute directly to the time-resolved emission. Figure 4 shows a comparison of the PL transients of CdS and CdS:Mn²⁺ nanoparticles at emission wavelengths 560 nm, 585 nm and 640 nm, corresponding to the three resolved gaussian peaks for CdS: Mn²⁺. It is observed that the PL decay of CdS:Mn²⁺, which is slower than that of the undoped samples upto the first ~ 15 ns., actually becomes faster subsequently. Earlier, Chung et al. made a similar observation for ZnS: Mn²⁺ nanoparticles [14]. However, Tanaka had reported a Mn²⁺ emission of ~ 1 ms in CdS:Mn²⁺ nanoparticles at room temperature [12], from which we could expect a substantial enhancement of CdS PL lifetime with Mn²⁺ doping. Clearly, even if such an enhancement occurs, it is not apparent in our results, possibly because the ~ 20 ns delay time is inadequate to detect the effect of a 1 ms time-constant. In other words, the effect of Mn²⁺ ions at a 1% doping

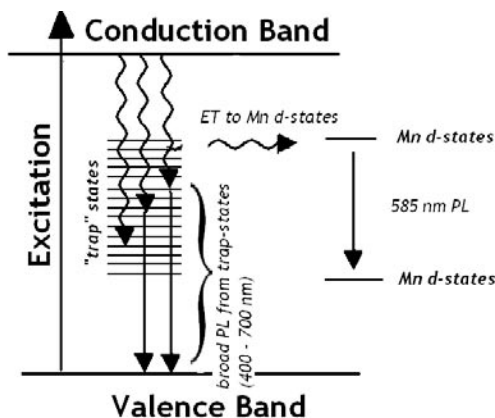


Fig. 5. Simplified scheme of excited state transitions taking place in doped CdS:Mn²⁺ nanoparticles.

level essentially perturbs the dynamics of the CdS trap-states, without directly contributing to the transient PL within the first ~20 ns delay time.

Conclusion

Doped and undoped CdS nanoparticles were successfully synthesized and stabilized in 0.05% PVP solutions in alcohols following a simple, wet-chemical technique. The absorption spectra show clear evidence of ~ 3 nm sized nanoparticle formation with strong quantum confinement effect. Steady-state and time-resolved photoluminescence studies help us to understand the excited state processes as illustrated in fig. 5. On excitation near the band-gap, the nanoparticles emit a broad photoluminescence covering 400 to 700 nm, originating predominantly from a heterogeneous population of trap-states. Even at 1% Mn²⁺ doping, the photoluminescence is significantly modified, with a new peak appearing at ~585 nm, attributed to the ⁴T₁-⁶A₁ transition of Mn²⁺ dopant states embedded in the CdS lattice. Time-resolved photoluminescence of CdS:Mn²⁺ nanoparticles suggest an energy transfer mechanism from the trap-states to the Mn²⁺

dopant atoms in the time-scale of ~1 ns (represented by the horizontal curved arrow in fig. 5). Although the photoluminescence dynamics of CdS nanoparticles is perturbed by 1% Mn²⁺ doping, the dynamics upto ~ 20 ns is dominated by the trap-states of CdS itself, with little or no direct emissive contribution from the dopant atoms.

Acknowledgements

Financial support for the work was obtained from the DST (Fast Track Project) and CSIR. The author gratefully acknowledges Prof. Kankan Bhattacharyya, Dept of Physical Chemistry, IACS, Kolkata, for the picosecond dynamics measurements conducted in his laboratory under the DST sponsored project IR/I1/CF-01/2002. Steady-state spectroscopy was performed in Visva-Bharati with instruments purchased under the DST (FIST program) and UGC (X th Plan program).

References

1. M. A. El-Sayed, *Acc. Chem. Res.* 37 (2004) 326.
2. P. N. Prasad, *Nanophotonics*, (John Wiley & Sons, Inc., New Jersey, 2004).
3. H. Yang and P. H. Holloway, *Appl. Phys. Lett.* 82 (2003) 1965.
4. W.C.W. Chan and S. Nie, *Science* 281 (1998) 2016.
5. X. Michalet, F.F. Pinaud, L.A. Bentolila, J.M. Tsay, S. Doose, J.J. Li, G. Sundaresan, A.M. Wu, S.S. Gambhar and S. Weiss, *Science* 307 (2005) 538.
6. M.A. Berg, R.S. Coleman and C.J. Murphy, *Phys Chem Chem Phys* 10 (2008) 1229.
7. J.R. Lakowicz, I. Gryczynski, Z. Gryczynski, and C.J. Murphy, *J. Phys. Chem. B* 103 (1999) 7613.
8. A. Schill and M. A. El-Sayed, *J. Phys. Chem. B* 108 (2004) 13619.

9. W.J. Parak, T. Pellegrino, C.M. Michael, D. Gerion, S.C. Williams and A.P. Alivisatos, *Nano Lett.* 3 (2003) 33.
10. D. Mandal and U. Chatterjee, *J. Chem. Phys.* 126 (2007) 103457.
11. A. Henglein, *Chem. Rev.* 89 (1989) 1861.
12. M. Tanaka, *J. Luminescence* 100 (2002) 163.
13. S. Sapra, A. Prakash, A. Ghangrekar, N. Periasamy and D.D. Sarma, *J. Phys. Chem. B* 109 (2005) 1663.
14. J.H. Chung, C.S. Ah and D.-J. Jang, *J. Phys. Chem. B* 105 (2001) 4128.



Debabrata Mandal completed his PhD under Prof. Kankan Bhattachayya at the Indian Association for the Cultivation of Sciences (IACS), Kolkata, in 2000. After a 2-year JSPS post-doctoral fellowship with Prof. Tahei Tahara at RIKEN, Japan, he joined Visva-Bharati University in 2003 as Lecturer in the Dept. of Chemistry. His research interests include the synthesis and spectroscopy of nanoparticles and nanocomposites.

Fluorescence studies on photoinduced intramolecular processes in homogeneous and biomimetic environments

Sivaprasad Mitra

Department of Chemistry, North-Eastern Hill University, Shillong – 793 022

E-mail: smitra@nehu.ac.in

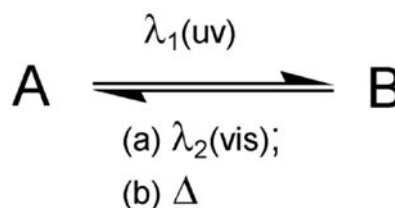
Some of the prototype intramolecular photo processes viz. charge transfer in covalently linked donor – acceptor systems and photoinduced intramolecular proton transfer in hydrogen bonded systems were probed in homogeneous medium as well as in cyclodextrin nanocavities by steady state and time resolved fluorescence spectroscopy. The difference in photophysical properties was discussed based on internal torsion, solvent polarity effect and preferential solubilization inside cyclodextrin cavities.

1. INTRODUCTION

Complex biological processes leading to life, their evolution and future existence can often be described and controlled by one or more *so called simple* chemical phenomena. Understanding of these processes, albeit their simplicity in isolated condition, is far from complete even today and more so when the systems are taken in relatively complicated biomimetic environment.

Intramolecular events are extremely important in chemistry and biology. There are quite a few well-characterized processes in nature [1]. These include rhodopsin isomerization in vision, light harvesting in the antenna complex of photosynthetic structures, electron transfer in photosynthetic reaction centers and some other examples involved in chemistry like keto – enol tautomerization, *cis – trans* isomerization, etc. It is often found that a particular process, which seems improbable under ordinary

chemical intuition, occurs easily in presence of light excitation and a reversible process between two entities, isomers (**A** & **B**) in many cases, having different absorption spectra, is initiated (scheme – I). The reverse process can either be modulated by another light (P-type) or in dark (T-type). So, the light acts as a source to activate the *chemical switch*.



Scheme – I Schematic diagram representing chemical switch

The primary feature common to the most of these systems is the extreme rapid rate under excitation in the gas phase as well as in nonpolar solvents where environmental perturbation is negligible. However, perturbations from solvent environment can modify the dynamics, which may either be prohibited within the excited-state life span or proceed with a prerequisite of solvent reorganization. The number and nature of the resulting species may also differ with the individual system under consideration and the medium concerned.

As the effect of light excitation produces completely different chemical structure, the physico-chemical properties

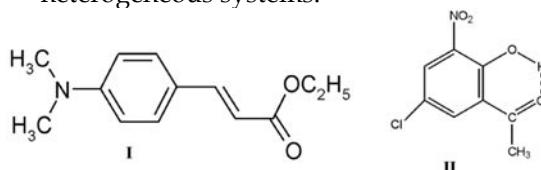
Table 1: Different photoinduced intramolecular processes and their application in technology and basic science

Process	Application
1. Intramolecular charge transfer (ICT)	(a) nonlinear optical material; (b) two photon absorbing chromophores; (c) electro-optical switches; and (d) chemical probes.
2. Tautomerization	(a) ESIPT laser; (b) special Raman filter; (c) switch for dye laser pulse shortening & conversion of solar into electrical energy; and (d) study of solvation dynamics, proton pumping & model system for DNA base pair.
3. <i>cis-trans</i> isomerization	(a) multimode chemical transducer; (b) paints/coatings for airplanes, land vehicles, submarines etc.; (c) photochromic glass & flash blindness goggles; and (d) information recording & data storage

of these systems in the excited state change abruptly. The drastic changes in physical and chemical properties of these systems in the excited state have often been exploited in technology as well as in basic science (table 1).

The large change in physical and chemical properties, strong solvent (medium) dependence of fluorescence behavior and appreciable change of some of the spectroscopically measurable quantities make these processes suitable for probing biological or bio-mimicking environment quite efficiently. Some of the common examples of photo-induced intramolecular processes include (a) facile intramolecular charge transfer (ICT) between covalently linked donor - acceptor systems; (b) keto - enol tautomerization of intramolecularly hydrogen bonded carbonyl compounds (ESIPT); (c) rapid isomerization of *trans* - azobenzene etc. In the present article, fluorescence studies involving photoinduced ICT in *trans*-Ethyl *p*-(dimethylamino) cinamate (I) and ESIPT of 2-acetyl-4-chloro-6-nitrophenol (II) (see scheme

- II, for structures) are presented both in homogeneous and as well as in constrained heterogeneous systems.



Scheme - II Structure of the compounds studied: *trans*-ethyl *p*-(dimethylamino) cinamate (I) and 2-acetyl-4-chloro-6-nitrophenol (II).

2. RESULTS & DISCUSSION

2.1. Photoinduced intramolecular charge transfer in *trans*-ethyl *p*-(dimethylamino) cinamate

Photoinduced intramolecular charge transfer (ICT) is the most widely studied phenomenon in the photophysics of donor (D) - acceptor (A) conjugated systems. *trans*-Ethyl *p*-(dimethylamino) cinamate (EDAC, I) is an efficient ICT probe which displays an intense absorption band around ~ 360 nm with a shoulder at 320 nm [2]. The vibrational structure observed for the long wavelength absorption band in cyclohexane is lost in

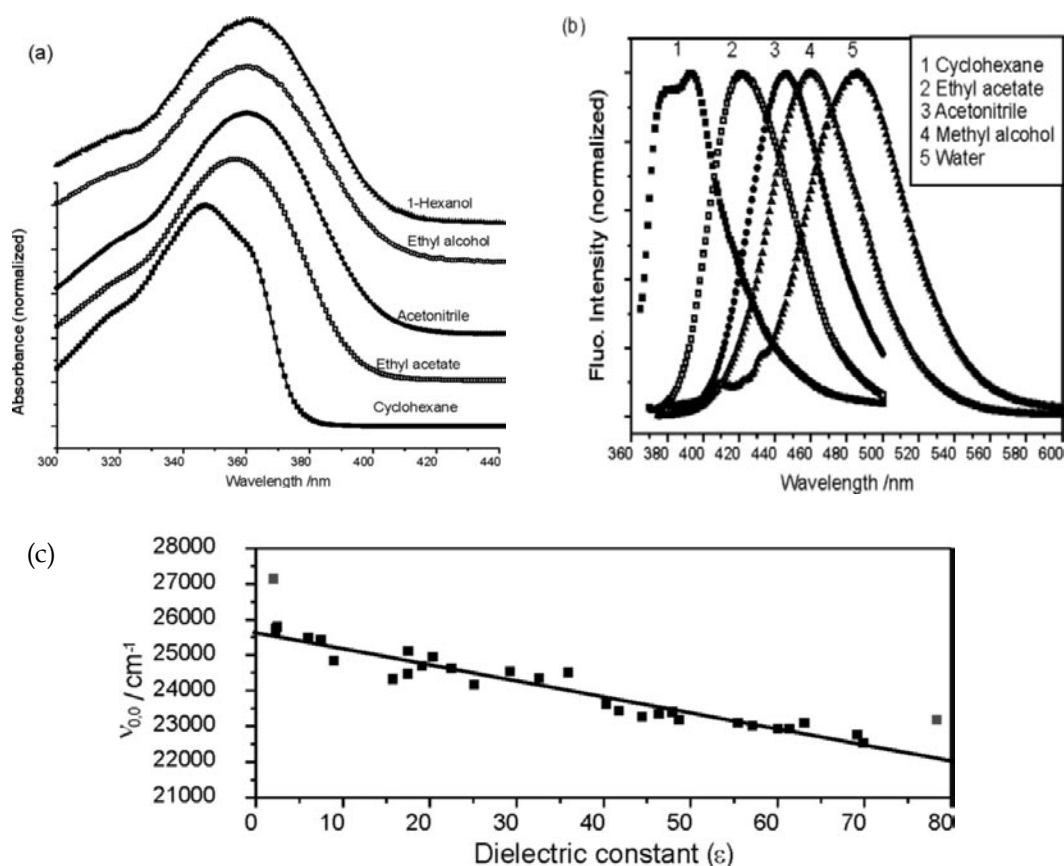


Fig. 1: Steady state absorption (a) and fluorescence emission (b) spectra of EDAC (**I**) in different solvents. The lower panel (c) shows the linear regression of 0,0 transition energy with static solvent dielectric parameter, ϵ as given in equation (1).

more polar solvents and spectral maxima shift to red with solvent polarity (figure 1a). However, the solvatochromic shift is rather small (~ 10 nm in acetonitrile relative to cyclohexane). In contrast, the fluorescence emission spectrum in cyclohexane with a maximum around 390 nm shows significant red shift with solvent polarity (~ 53 nm in acetonitrile relative to cyclohexane), which indicates the strong charge transfer character of the fluorescent state in polar solvents (figure 1b). The dipole moment of locally excited ($\mu_{LE} \sim 6.7$ D) and charge transfer

($\mu_{CT} \sim 12$ D) states were estimated from the slope of the plots of absorption (ν_a) and fluorescence (ν_f) energies against the solvent polarity parameter, $\Delta f(\epsilon, n)$, respectively. The energy of the 0,0 transition ($\nu_{0,0}$, the intersection of normalized absorption and emission spectra) shows very good correlation with solvent static dielectric constant, ϵ over a wide range of protic and aprotic solvents as given in equation (1)

$$\nu_{0,0} / \text{cm}^{-1} = (25628.24 \pm 92.4) + (-45.1 \pm 2.3) \times \epsilon; R = 0.99 \quad (1)$$

The deviation (figure 1c) in cyclohexane is due to the different nature of emission (LE type) when compared with other solvent systems (ICT type), while, the large deviation in aqueous medium may be due to extra stabilization of the highly polar ICT state in extensive hydrogen bonded network of water cluster [3].

The fluorescence quantum yield (ϕ_f) and decay time (τ_f) corresponding to the ICT emission of **I** have been determined in a variety of solvents. All decays could be reproduced with single exponential decay function. Radiative (κ_f^r) and non-radiative (κ_f^{nr}) decay rate constants were calculated from the known value of fluorescence quantum yield (ϕ_f) and decay time (τ_f). It is seen from table 2 that the magnitude of κ_f^{nr} is much higher than κ_f^r . Low fluorescence quantum yield and the short excited state fluorescence decay time of **I** in solutions are direct indications of the nonradiative processes being dominant in the excited state photophysics.

The early time dynamics of photophysical processes of **I** in some of the solvents were studied using ultrafast transient absorption experiments. The

results indicate that the LE state converts into the ICT state within 350 ± 100 fs. A combination of solvent reorganization and intramolecular vibrational relaxation within 0.5~6 ps populates the relaxed ICT state [4].

Complexation behavior of **I** was also monitored with both α - and β -cyclodextrins (CD) at different solution pH. The absorption peak position at 360 nm shows bathochromic shift of about 8~10 nm in CD environment. However, the ICT fluorescence characteristics of **I** in aqueous solutions at different pH are seen to undergo drastic changes in presence of cyclodextrins (figure 2). In all the cases, the fluorescence intensity increases with increase in CD concentration and then saturates to a limiting value. In addition, the fluorescence spectra also show gradual blue shift on increasing concentration of CD. In presence of ~5 mM β -CD, the fluorescence emission peak of **I** ($\lambda_{max} = 465$ nm) shifts about 20 nm as compared to that observed in pure aqueous solution ($\lambda_{max} = 485$ nm). All these results also point towards the formation of EDAC-CD complex. Benesi-Hilderbrand (BH) analysis of the EDAC-CD complexation data confirm that EDAC forms 1:1 complex

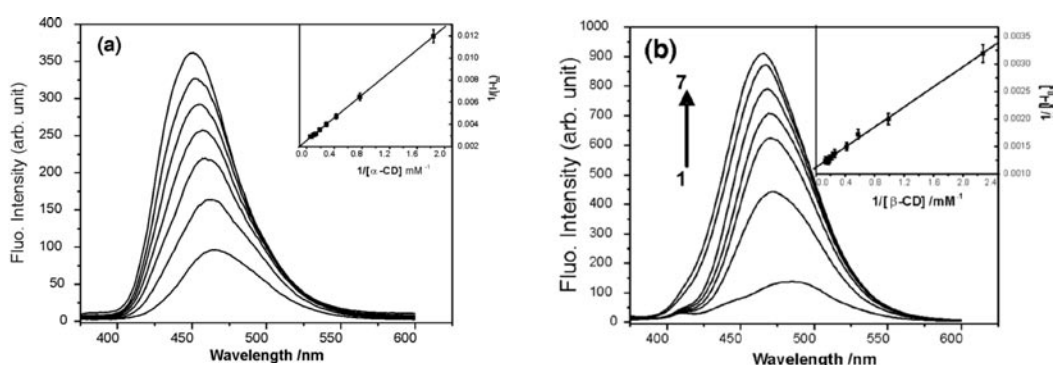


Fig. 2: Fluorescence emission spectra of **I** ($1.2 \times 10^{-5} \text{ mol dm}^{-3}$) with increasing concentration of α -cyclodextrin at pH = 2.8 (a) and β -cyclodextrin at pH = 9.2 (b). Inset shows the double reciprocal plot for 1:1 complex formation in the respective cases.

Table 2: Fluorescence quantum yield (ϕ_f), decay time (τ_f), radiative (κ_f^r) and nonradiative (κ_f^{nr}) decay rate constants of EDAC (I) in different solvents

Solvent	ϕ_f /10 ⁻³	τ_f /ps	κ_f^r /10 ⁸ s ⁻¹	κ_f^{nr} /10 ¹⁰ s ⁻¹
Cyclohexane	6.0	-	-	-
Benzene	11.3	39	2.9	2.5
Toluene	11.9	58	2.1	1.7
Ethyl acetate	15.1	23	6.6	4.3
1,4-Dioxane	14.0	30	4.7	3.3
Tetrahydrofuran	12.1	69	1.8	1.4
Acetonitrile	22.0	101	2.2	1.0
Water	3.2	90	0.4	1.1
Methanol	6.5	75	0.9	1.3
Ethanol	5.7	82	0.7	1.2
1-Propanol	4.3	89	0.5	1.1
1-Butanol	4.0	110	0.4	0.9
1-Hexanol	3.9	118	0.3	0.8
1-Octanol	3.1	129	0.2	0.7

Table 3: Binding constant (K) of 1:1 complex of EDAC (I) with α - and β -cyclodextrin at different pH

pH	α -CD	β -CD
2.8	498	579
7.2	177	1970
9.2	246	1224

with both α - and β -cyclodextrin in varying experimental pH. However, the equilibrium constant (K) values calculated from the slope and intercept indicate that **I** penetrate more towards the cyclodextrin cavity in the later (table 3). Since EDAC is approximately 5.1 Å in width [4], it should fit perfectly in β -CD, having cavity diameter of 6.0~6.5 Å [5]. On the other hand, the diameter of 4.7~5.3 Å in α -CD is not suitable for formation of proper

host-guest complex due to very strong van der Waals interaction.

However, the K values are comparable at pH ~ 2.8 for both α - and β -cyclodextrins. As discussed earlier [2], at this experimental pH, **I** remains mainly in the protonated state on the dimethylamino group. Penetration of charged dimethyl amino group is not favored inside the hydrophobic CD cavity. Consequently, a very weak complex is formed with both α - and β -CDs under this condition.

2.2 ESIPT in 2-acetyl-4-chloro-6-nitrophenol

The absorption spectrum of 2-acetyl-4-chloro-6-nitrophenol (**II**) in nonpolar solvent shows a single peak around ~355 nm. However, the fluorescence emission spectrum corresponding to this absorption consists of two bands. The high energy, structured emission at around 430 nm has less Stokes shift ($\Delta\nu_{ss} \sim 5000 \text{ cm}^{-1}$) compared to that of the broad, low energy, unstructured emission at 505 nm having unusually large Stokes shift ($\Delta\nu_{ss} \sim 8300 \text{ cm}^{-1}$). The excitation spectra corresponding to both these emissions match very closely to the ground state absorption spectra and appear at about 375 and 360 nm, respectively.

In accordance to the previous studies for ESIPT in *o*-hydroxy acetophenone derivative, the largely Stokes shifted emission arises due to the proton transfer (ESIPT fluorescence) in $S_1(\pi\pi^*)$ state of primary enol (**E**) form, where the intramolecular hydrogen bond involves the phenolic hydrogen and carbonyl oxygen of acetyl group in the *ortho* position (structure (a), figure 3) to form the keto (**K**) conformer (structure (b)). On the other hand, the structured emission with less $\Delta\nu_{ss}$ value may arise from another conformer of the enol structure where the hydrogen

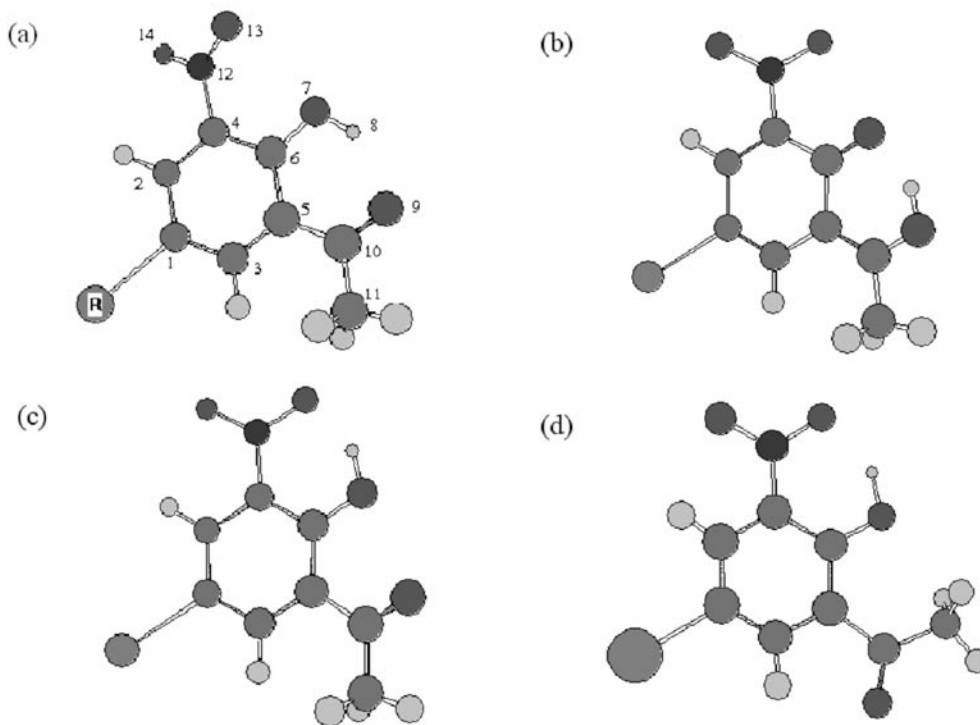


Fig. 3: Optimized structures of different possible conformers of **II** ($R = Cl$) at TDDFT/6-31++G(d,p)//HF/6-31G(d,p) level of calculation. Enol (a), Keto (b) and non-ESIPT enol structures (c) and (d) are represented in text as **E**, **K**, **E1** and **E2**, respectively. Numbering scheme used during ab-initio calculations is also shown.

bonding partners involve the phenolic hydrogen and oxygen of the nitro group in the *ortho* position. As shown in figure 3, two structural forms can be presumed for this conformer (**E1** and **E2**, structures (c) and (d), respectively). However, from the geometry of these two conformers, it is seen that in **E1** the proximity of oxygen atoms in neighboring acetyl and phenolic groups may cause additional non-bonding interaction. Therefore, relative abundance of **E2** should be more in the solution compared to **E1**. Theoretical calculation indeed predicts in the same line. On the other hand, relative energy difference, as obtained from DFT calculation, between **E** and **E2** structures vary from 0.5 ~ 0.02 kcal mol⁻¹ in different solvents studied here. Very

small energy difference in solution indicates that there is equilibrium among different enol conformers in the ground state and ESIPT emission from **E** is in competition with normal fluorescence from **E2**.

The calculated excited state energy difference between **E** and **E2** is ~5.6 kcal mol⁻¹ in CCl₄ and decreases substantially to 3.5 kcal mol⁻¹ in polar solvents like ethanol or acetonitrile. The large energy difference in nonpolar solvent ensures the ground state equilibrium between these structures to be perturbed in the excited state and respective emission appears from individual conformers [6]. However, the situation is different in polar solvents and needs to be discussed in more detail. The interaction

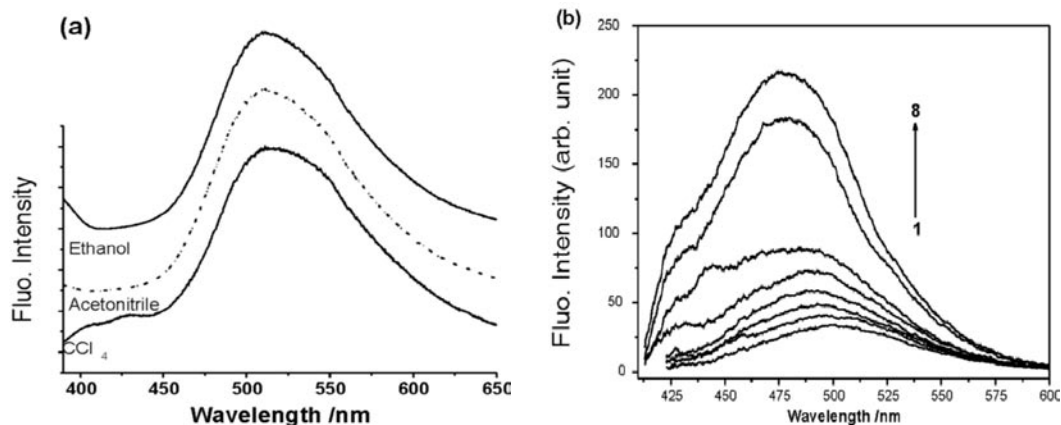


Fig. 4: Fluorescence emission spectra of **II** in different solvents (a) and with increasing concentration of added β -cyclodextrin in aqueous solution (b). $[\beta\text{-CD}]/\text{mM} = 1(0.0), 2(2.2), 3(3.6), 4(4.9), 5(6.8), 6(9.0), 7(17.6)$ and $8(22.2)$, respectively.

of excited fluorophore and solvent dipole reduces the energy difference substantially. Furthermore, ESIPT is known to be a very efficient nonradiative deactivation channel for intramolecularly hydrogen bonded compounds and occurs in ultrafast time scale [7,8]. Also, the keto conformer (**K**) is the most stable geometrical entity in the excited state. So, it is reasonable to argue that ESIPT acts both as a thermodynamic and kinetic sink in the excited state potential energy surface and the equilibrium is tilted heavily towards the pro-ESIPT conformer (**E**) in these solvents for **II**. As a result, the fluorescence spectra show only ESIPT emission at around ~ 510 nm in these solvents.

The argument on the difference in photophysical properties of **II** in polar solvents to that in non-polar solvents like CCl_4 can further be substantiated by observing the fluorescence spectra of the probe encapsulated in cyclodextrin nanocavities. As the host cavities render relatively more hydrophobic environment to the probe, it is expected that the ESIPT fluorescence of **II** in pure water will be

changed to both ESIPT and non-ESIPT fluorescence under encapsulation with CDs. As shown in figure 4, this is indeed the observation in presence of CDs.

In conclusion, the fluorescence behavior of representative intramolecular processes, viz. ICT and ESIPT was monitored in *trans*-ethyl *p*-(dimethylamino) cinamate and 2-acetyl-4-chloro-6-nitrophenol, respectively in homogeneous media as well as in cyclodextrin nanocavities. It was found that preferential solubilization inside cyclodextrin cavities, solvent polarity and also the internal torsional motion are important controlling factors for the difference in environment dependent fluorescence behavior. These motions are integral components for construction, stability and function of macromolecular architecture.

Acknowledgement:

The author thanks DST and CSIR for funding through research grants SR/FTP/CS-38/2004 and 01(1975)/05/EMR - II, respectively.

References:

1. Coyle, J.D.; Hill, R. R.; Roberts, D. R. (Eds.) *Light, chemical change and life*, Milton Keynes, 1982.
2. Singh, T. S.; Mitra, S. J. *Lumin.* 2007, 127, 508.
3. Singh, T. S.; Mitra, S. J. *Colloid and Interface Sci.* 2007, 311, 128.
4. Singh, T. S.; Mitra, S.; Chandra, A. K.; Tamai, N.; Kar, S. J. *Photochem. Photobiol. A:Chem.* 2008, 197, 295.
5. Szejtli, J. *Chem. Rev.* 1998, 98, 1743.
6. Mitra, S.; Singh, T. S.; Mandal, A.; Mukherjee, S. *Chem. Phys.* 2007, 342, 309.
7. Lochbrunner, S.; Wurzer, A. J.; Riedle, E. J. *Phys. Chem. A* **2003**, 107, 10580.
8. Rini, M.; Kurnmrow, A.; Dreyer, J.; Nibbering, E.T.J.; Elsaesser, T. *Faraday Discuss.* **2002**, 122, 27.



Dr. Sivaprasad Mitra received his Ph.D. degree in 1997 from Dept. of Physical Chemistry, IACS. He visited Kwansai Gakuin University (JSPS fellow, 1997-1999) and Katholieke University of Leuven (Belgium, 1999-2001) during his post-doctoral research with Professor N. Tamai and Professor F. C. De Schryver, respectively. After a short stay at TIFR with Dr. S. Maiti as a visiting fellow, he joined as a lecturer in the Dept. of Chemistry, BITS, Pilani. Since 2003, he moved in the Chemistry Dept., NEHU, Shillong. His current research interests focus on fluorescence spectroscopy in homogeneous as well as microheterogeneous environments.

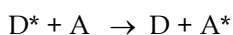
Fluorescence resonance energy transfer: A spectroscopic ruler

Deboleena Sarkar, Paramita Das and Nitin Chattopadhyay*

Department of Chemistry
Jadavpur University, Kolkata – 700032.
E-mail: nitin.chattopadhyay@yahoo.com

Introduction

A fundamental difference between a ground state species and its photoexcited counterpart is that the latter possesses some amount of energy over the former. The photoexcited states are really metastable states and the excited species can not stay there for long. In course of time the excited species comes down to its ground state through dissipation of the excess energy. There are number of ways that the excited species may follow for its deactivation. Energy transfer (ET) is one of the most efficient routes in the category. Upon interaction with a suitable acceptor or quencher (A) the excited fluorophore (D*) can be deactivated through transferring its energy to the former. The overall process may be described as



Presence of the quencher, thus, results in a decrease in the fluorescence from the fluorophore. D* is known as *excitation donor* or *energy donor* while A is called *excitation acceptor* or *energy acceptor*. The singlet-singlet energy transfer involves two types of interactions, exchange interaction and coulombic interaction. Exchange interaction occurs via overlap of the electron clouds and thereby requires physical contact between the interacting partners. Coulombic resonance interaction or simply coulombic interaction occurs via the electromagnetic field and does not require a physical contact. Induction of the dipole oscillation plays

the role in the latter type of interaction. A major distinction between the exchange mechanism (also called *collision mechanism*) and the coulombic mechanism (also called *induced dipole mechanism*) is that the former requires collision while the latter does not. In other words, in exchange mechanism the energy is transferred from the fluorophore to the quencher in an analogous way as a moving particle transfers momentum to other particles with which it collides. In the coulombic mechanism the energy is transferred to the quencher through space.

Fluorescence resonance energy transfer (FRET) or *resonance energy transfer* (RET) is typically a distance dependent, through space energy transfer process in which the excitation energy is transferred from the excited fluorophore (D*) to the unexcited acceptor (A) through induced dipole mechanism. The fluorescence from the donor molecule is basically absorbed by the acceptor molecule resulting in the non-appearance of a photon from the donor fluorophore. The rate and efficiency of FRET process depends upon (i) fluorescence quantum yield of the donor, (ii) the absorbance of the acceptor molecule in the specific wavelength region, (iii) extent of spectral overlap between the fluorescence spectrum of the donor and the absorption spectrum of the acceptor, which is theoretically related to the density and probability of isoenergetic resonance transitions from various vibrational levels for the $D^* + A \rightarrow D + A^*$ process, (iv) the relative orientation of the transition dipoles

of the donor and the acceptor and (v) the distance between the donor and the acceptor molecules. It is pertinent to mention here that the rate constant as well as efficiency of FRET depends on the inverse sixth power of the distance between the donor and the acceptor moieties. This sensitivity in the distance dependence of FRET enables one to exploit the photoprocess for measuring distances between donors and acceptors in different situations. The ability to determine the donor-acceptor separation has termed the FRET process as “spectroscopic ruler”. The most common application of FRET is to measure the distance between two sites on a macromolecule like polymer, protein, DNA etc. For protein systems, the tryptophan residue of the protein is often used as the donor. External donors are also employed in other cases. The technique is often used in biochemical research.

Theoretical Backdrop:

The theoretical ground for FRET, developed from both the classical and quantum mechanical considerations, is moderately complex. According to the classical theory, the interaction energy, E, between two electric dipoles is related to the magnitude of the two dipoles (μ_A and μ_D) and the distance between them (R_{DA}) leads to the following equation¹:

Interaction Energy, E (dipole-dipole)

$$\propto \frac{\mu_D \mu_A}{R_{DA}^3} \dots\dots\dots(1)$$

μ_A and μ_D are assigned to the oscillator strengths for radiative transitions $A \rightleftharpoons A^*$ and $D^* \rightleftharpoons D$ respectively. Since rate of energy transfer (k_{ET}) following the dipole-dipole mechanism is related to E^2 , and E^2 is related to experimental properties, Förster showed that k_{ET} can be related to E^2 as follows¹:

$$k_{ET} \text{ (Coulombic)} \rightarrow E^2 \sim \left(\frac{\mu_D \mu_A}{R_{DA}^3}\right)^2 = \frac{\mu_D^2 \mu_A^2}{R_{DA}^6} \dots\dots(2)$$

Thus, Förster’s theory predicts that k_{ET} for an energy transfer process via coulombic interaction will be proportional to: (a) square of the transition dipole moment μ_D , (b) the square of the transition dipole moment μ_A , and (c) the inverse sixth power of the separation between D^* and A.

The transition dipole moments can be derived experimentally as:

$$\mu_D^2 (D^* \rightleftharpoons D) \rightarrow \int \epsilon_D(\lambda) d\lambda \text{ or } k_D^0$$

$$\mu_A^2 (A^* \rightleftharpoons A) \rightarrow \int \epsilon_A(\lambda) d\lambda \text{ or } k_A^0$$

where $\int \epsilon(\lambda) d\lambda$ is the integrated extinction coefficient of the corresponding absorption band and k^0 is the pure radiative rate constant of the species denoted by the subscripts.

For the specific energy transfer process $D^* \rightarrow D$ and $A \rightarrow A^*$, substituting k_D^0 and $\int \epsilon_A$ as the experimental terms in place of μ_D^2 and μ_A^2 respectively in equation (2), we get the final equation as

$$k_{ET} \text{ (Coulombic)} \rightarrow \frac{k_D^0 \int \epsilon_A(\lambda) d\lambda}{R_{DA}^6} \dots(3)$$

Again, considering the overlap of emission of D^* with the absorption of A, we get a further modified form of the above equation as,

$$k_{ET} \text{ (Coulombic)} = k \frac{\kappa^2 k_D^0}{R_{DA}^6} J(\epsilon_A) \dots(4)$$

k is a constant that takes care of the experimental conditions such as the refractive index of the medium. κ^2 refers to the orientation between the two interacting dipoles. κ^2 is taken to be equal to 2/3 for a random distribution of the dipoles². The term $J(\epsilon_A)$ describes the overlap integral including in it the extinction coefficient of the acceptor as²:

$$J(\epsilon_A) = \int_0^\infty F_D(\lambda) \epsilon_A(\lambda) \lambda^4 d\lambda \quad \dots(5)$$

where, $F_D(\lambda)$ is the corrected fluorescence intensity of the donor at wavelengths λ to $(\lambda+d\lambda)$ with the total intensity normalized to unity and $\epsilon_A(\lambda)$, the molar extinction coefficient of the acceptor at wavelength λ .

Experimentally, it is conventional to measure the *efficiency* and not the *rate constant* of the energy transfer process under discussion¹. This is because, it is convenient to typify an efficiency for which the rate of energy transfer (k_{ET}) is equal to the sum of the rates of deactivation of D^* .

$$k_{ET}[D^*] [A] = k_D[D^*] \quad \text{at } R = R_0$$

or

$$k_{ET}[A] = k_D = 1 / \tau_D$$

k_D is the inverse of the experimental lifetime of D^* , not the theoretical rate constant (k_D^0). R_0 is defined as the Förster distance or *critical separation* between donor and acceptor at which the transfer rate (k_{ET}) is equal to the decay rate of the donor in the absence of the acceptor $(1/\tau_D)^2$.

The rate constant and the efficiency of an energy transfer process can be related to actual donor-acceptor separation (R) according to the following expressions¹:

$$\text{Rate: } k_{ET} \propto k_D \left(\frac{R_0}{R}\right)^6 = \left(\frac{1}{\tau_D}\right) \left(\frac{R_0}{R}\right)^6 \quad (6)$$

$$\text{Efficiency: } \Phi \propto \left(\frac{R_0}{R}\right)^6 \dots\dots\dots (7)$$

In this case, τ_D describes the mean lifetime of D^* and Φ is the quantum yield of energy transfer. Hence, when $R = R_0$, $k_{ET} = 1 / \tau_D$. If $R < R_0$, there occurs a highly favorable transfer of energy whereas if $R > R_0$, D^* gets

deactivated via other routes. The energy transfer efficiency is typically measured by relative fluorescence intensity of the donor, in the absence (F_D^0) and in the presence (F_D) of the acceptor as

$$\Phi = 1 - \frac{F_D}{F_D^0} = 1 - \frac{\tau_D}{\tau_D^0} \quad \dots(8)$$

The above equation is applicable to donor-acceptor pairs separated at a fixed distance, a situation often encountered with labeled proteins.

Measurement of distance using FRET in different environments

Because rate and / or efficiency of FRET depends on the inverse sixth power of the separation between the donor and the acceptor ($1/R^6$), the process can be exploited to measure the distance between two sites. Therefore the process of FRET is aptly coined as a '*spectroscopic ruler*'. It is basically a distance dependent interaction between the different electronic excited states of probe molecules in which the excitation energy is transferred from one molecule (donor) to another molecule (acceptor) without emission from the former molecular system. FRET is an important technique for investigating a variety of biological phenomena including energy transfer processes. One important consequence of energy transfer is photosensitization, a classic example of which is photosynthesis. Also FRET plays a key role in photodynamic therapy (PDT) and is extensively used to study the structure, conformation, spatial distribution and assembly of complex proteins. Furthermore, in a proteinous environment the proximity of a guest molecule to the tryptophan moiety is often determined through FRET study.

According to the Förster's non-radiative energy transfer theory³, the energy transfer efficiency Φ depends not only on the distance (R) between the donor and the acceptor, but also on the critical energy transfer distance (R_0) expressed by the following relation

$$\Phi = R_0^6 / (R_0^6 + R^6) \dots\dots\dots (9)$$

where R_0 is the characteristic distance, called the Förster's distance or critical distance, at which the efficiency of transfer is 50%. The magnitude of R_0 is dependent on the spectral properties of the donor and the acceptor molecules¹. R_0 is expressed in Å as follows

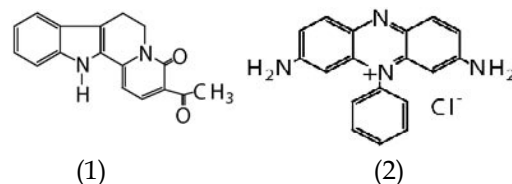
$$R_0^6 = 8.8 \times 10^{23} [\kappa^2 n^4 \phi_D J(\epsilon_A)] \dots\dots\dots (10)$$

where κ^2 , as discussed above is the factor expressing the relative orientation of the donor to the acceptor molecule, n is the refractive index of the medium, ϕ_D is the quantum yield of the donor in the absence of the acceptor and $J(\epsilon_A)$ is the overlap integral of the fluorescence emission spectrum of the donor and the absorption spectrum of the acceptor as has already been defined in equation (5). With knowledge of the energy transfer efficiency (Φ) and the critical energy transfer distance (R_0), the distance (R) between the donor and the acceptor molecule can be easily calculated using relation (9). Here we offer some specific examples in different environments to exploit the "spectroscopic ruler".

In homogeneous environment

Fluorescence resonance energy transfer has been studied in water between 3-acetyl-4-oxo-6,7-dihydro-12H indolo-[2,3-a]quinolizine (AODIQ) and phenosafranin (PSF) (Scheme 1), the former one being a non-ionic fluorophore while the latter one is a cationic dye. Phenosafranin is one of the popular phenazinium dyes, used as a

sensitizer in energy and electron transfer reactions in homogeneous media and in semiconductors⁴. AODIQ is an established bioactive molecule⁵. Here AODIQ serves as the donor while PSF serves as the acceptor for the energy transfer process.



Scheme 1— Structures of (1) AODIQ and (2) PSF

The fluorophore, AODIQ shows a broad absorption band at 420 nm and yields an unstructured, charge transfer (CT) emission band in aqueous solution with maximum at 520 nm⁵. In aqueous medium, a broad absorption band of PSF with a maximum at 520 nm is observed with a corresponding CT fluorescence appearing with a maximum at 585 nm⁴. Considering the fact that PSF absorbs mostly at a region where AODIQ emits, the fluorophores are judged as a promising pair for the FRET study (Fig.1).

Insignificant direct excitation of PSF at 420 nm in the blank experiment confirms the occurrence of the FRET process between the chosen pair. In aqueous solution of AODIQ, gradual addition of PSF leads to a quenching of the AODIQ fluorescence at 520 nm with the concomitant generation of a new band through an isoemissive point at 566 nm (Fig.2). During the FRET study, no additional band is observed at longer wavelength in the fluorescence spectrum of the mixture of donor and acceptor. This negates the possibility of the exciplex formation between the photoexcited donor and the acceptor molecules².

For a FRET process it is important to read the process through a measure of

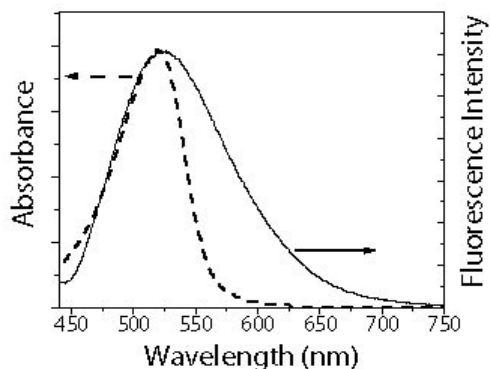


Fig.1: Overlap of absorption spectrum of PSF (dotted line) with emission spectrum of AODIQ (solid line) in aqueous solution.

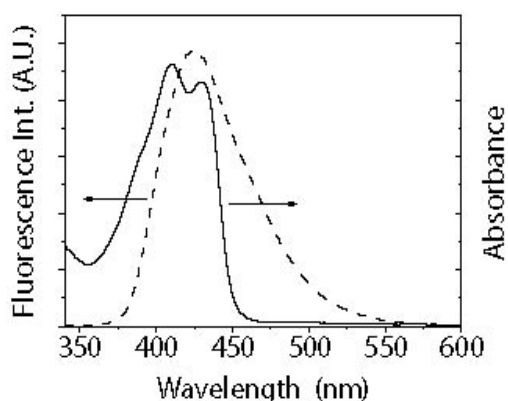


Fig.2. Fluorescence spectra of AODIQ (7 μM) as a function of PSF concentration ($\lambda_{\text{exc}} = 420 \text{ nm}$). For curves (i) \rightarrow (ix), PSF concentrations are 0, 1.0, 3.0, 5.4, 7.0, 10, 16.7, 22.4 and 31 μM .

the energy transfer efficiency (Φ). Energy transfer efficiency Φ has been determined to be 0.39 at 1:1 condition of donor-acceptor pair using equation (8). The value of critical energy transfer distance (R_0) depends on the spectral properties of both the donor and the acceptor molecular systems and it has been calculated to be 75 Å using the relation (10). Knowing the values of Φ and R_0 , using equation (9) the distance between the donor and the acceptor, R is found to be 81 Å in

aqueous solution. An estimate of R can be had from the dimensions and concentrations of the acceptor molecules using nearest neighbor distribution.

A parallel experiment was also conducted with the same probe AODIQ but now exploiting it as an acceptor and a newly synthesized substituted coumarin derivative 7-hydroxy-4-methyl-8-(4'-methylpiperazine-1'-yl)methylcoumarin (HMMC) as donor in dioxane solvent⁶. The fact that these two can serve as promising pairs for FRET is evidenced from the good overlap between the absorption spectrum of AODIQ and the fluorescence spectrum of HMMC as depicted in Fig. 3.

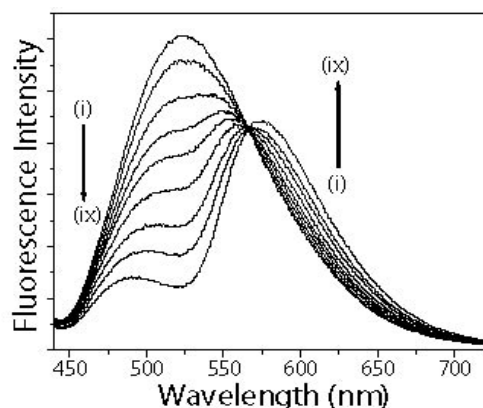


Fig. 3: Overlap of absorption spectrum of AODIQ (solid line) and fluorescence spectrum of HMMC (broken line). In both the cases the solvent is dioxane.

The Förster distance (R_0) has been calculated assuming random orientation of the donor and acceptor molecules. Taking $\kappa^2 = 2/3$, $n = 1.422$, $\phi_D = 0.56$ and with the help of the relation (10) it was found to be 24.9 Å. The sum of collision radii of donor (HMMC) and acceptor (AODIQ) is about 12-13 Å. The significant difference between the values of the collision radii (12-13 Å)⁶ and the critical radius of energy transfer (24.9 Å) suggests

that for HMMC-AODIQ pair a long range dipole - dipole interaction is responsible for the energy transfer mechanism⁶⁻⁸. The energy transfer efficiency (Φ) for the pair of HMMC and AODIQ in case of 1:1 composition has been calculated and is found to be 0.33. From the value of the energy transfer efficiency (Φ) and the critical energy transfer distance (R_0) for 1:1 composition, the distance (R) between the donor and acceptor molecule has been calculated to be 28 Å using relation (9).

In micellar environment

Owing to the great potential of FRET studies researchers have investigated different aspects of this process in organized environments formed by surfactants, i.e., micelles and reverse micelles. Most of these studies on energy transfer have been performed taking the donor and acceptor molecules (external) solubilized in such environments. However, very few reports have appeared so far where the surfactant itself serves as the donor unit. The present example draws attention in this regard. Use of non-ionic surfactant triton X-100 (TX-100), rules out the involvement of electrostatic interaction in the energy transfer process. Critical micellar concentration (CMC) of TX-100 is reported to be around 0.30 mM. The acceptor 3-acetyl-4-oxo-6,7-dihydro-12H indolo-[2,3-a] quinolizine (AODIQ), a neutral molecule, used in the present experiment has already been shown to be an excellent fluorescent probe for biological systems. Given the broad range of biological activities of AODIQ and TX-100 we became interested in the FRET studies between nonionic surfactant TX-100 acting as donor and solubilized AODIQ acting as the acceptor. The present study covers both pre-micellar and micellar environments to see the effect of micellization on the energy transfer process⁷.

Phenyl group present in TX-100 absorbs appreciably at 270 nm giving a somewhat broad fluorescence peaking at 300 nm. As already stated, AODIQ shows a broad CT emission with a maximum at 520 nm in aqueous medium. In TX-100 environment, however, this band maximum is blue shifted to 488 nm⁹. Considering the fact that AODIQ has appreciable absorption at a wavelength range where TX-100 emits, the pair was judged as a good pair of donor-acceptor system for the FRET study (Fig. 4).

In an aqueous solution of TX-100 (in both pre-micellar and micellar concentrations) gradual addition of AODIQ leads to a decrease in the intensity of the fluorescence of TX-100 with a concomitant increase in the fluorescence of AODIQ. An isoemissive point appears at 422 nm (Fig. 5). That the AODIQ fluorescence is originating through FRET and not from the directly excited fluorophore molecules was confirmed from a comparison of the total fluorescence coming from the mixtures of donor and acceptor to that coming from the blank experiments with the acceptor AODIQ only having the same concentration⁷.

Absence of any additional absorption band and any additional new band in the emission spectrum at longer wavelengths evidence against the formation of any ground-state complex or exciplex between the donor (photoexcited) and the acceptor molecules in solution^{2,6-8}.

The quenching of the fluorescence of the donor (phenyl group of TX-100) with the addition of acceptor (AODIQ) in both pre and post CMC conditions of the surfactant were followed by Stern-Volmer relation:

$$F_0 / F = 1 + K_{sv} [Q] \dots\dots\dots (11)$$

where F_0 , F are fluorescence intensities of donor in the absence and in the presence of acceptor molecule respectively, $[Q]$ is the quencher (here acceptor) concentration.

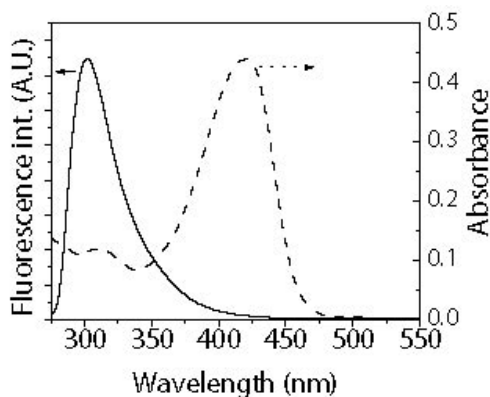


Fig. 4: Overlap of fluorescence spectrum of TX-100 (solid line) and absorption spectrum of AODIQ (dotted line) in aqueous medium.

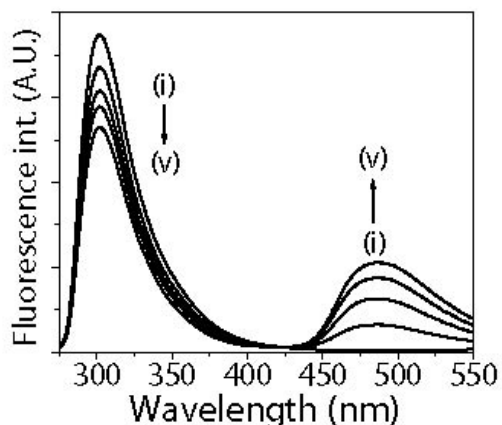


Fig. 5 Fluorescence spectra of TX-100 (1 mM) as a function of AODIQ concentrations ($\lambda_{exc} = 270$ nm). For curves (i) \rightarrow (v), AODIQ concentrations are 0, 4.85, 9.75, 14.55 and 24.25 μ M.

From Fig. 6 it is evident that the Stern-Volmer plot is linear in the concentration range of the acceptor studied. The linearity of this plot indicates only one type of quenching². As discussed above, from the absence of any additional absorption band in the donor-acceptor mixture the possibility of ground state complex formation is ruled out and the quenching is rationalized in terms of energy transfer. From the slope of the curve, quenching rate constant (K_{SV})

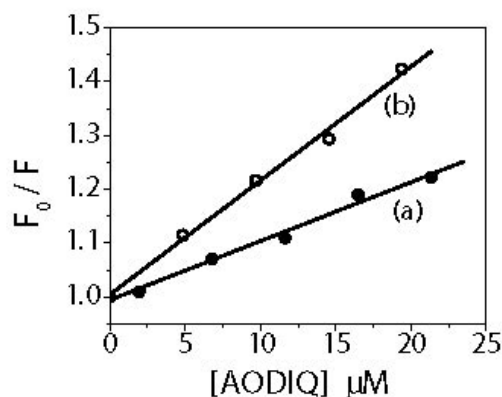


Fig. 6: Stern-Volmer plots for the quenching of TX-100 by AODIQ in (a) pre-micellar (0.1 mM) and (b) post CMC (1.0 mM) domain.

values were determined in pre-micellar ($[TX-100] = 0.1$ mM) and micellar ($[TX-100] = 1.0$ mM) situations and they were 1.1×10^4 ML^{-1} and 2.1×10^4 ML^{-1} respectively. The determined K_{SV} values fall in the normal range reported earlier for similar type of FRET reactions⁸ and are order of magnitude higher than that observed for a normal diffusion controlled quenching process. The observation suggests that the dominant mechanism of fluorescence quenching is the resonance energy transfer through long-range dipole-dipole interaction rather than the simple diffusion limited process between the excited donor and the ground state acceptor molecules.

As in the previous citation an attempt was made in this case too to determine the energy transfer efficiency. The energy transfer efficiency in both pre CMC ($[TX-100] = 0.1$ mM) and post CMC condition ($[TX-100] = 1.0$ mM) for a common acceptor concentration (20 μ M) have been determined and it is found that the efficiency in the micellar environment (0.27) is remarkably higher than that in the pre-micellar situation (0.16). An increase in the energy transfer efficiency in the micellar environment

compared to that in the pre-micellar situation is rationalized from the consideration of the formation of the micellar aggregates. Before micelle formation, the surfactant units remain in a rather scattered and unorganized pattern. At TX-100 concentrations above the CMC, micellar units are formed. It has already been established that in TX-100 micellar medium AODIQ molecules locate themselves mostly near the micelle-water interface region⁹. This leads to the proximity of the phenyl group of TX-100 and the donor AODIQ, resulting in making the energy transfer process more efficient.

With an estimate of the energy transfer efficiency and the critical energy transfer distance (R_0), the distance (R) between the donor and acceptor molecule may be calculated using equation (9). However in this case, fluorescence quantum yield of the donor, which is involved in calculating the distance from the FRET technique, depends remarkably on the concentration of the surfactant in the medium. An uncertainty in the fluorescence quantum yield, thus, makes determination of the distance between the energy transfer partners meaningless. Under the situation, no attempt was made to determine R experimentally⁷. The high value of K_{sv} , however, suggested that this distance might be much larger than the micellar dimensions.

A similar attempt has been made by De *et al.*¹⁰. For their study the pairs that have been used are fluorescein with Nile red and acridine orange with Nile red in micelles and reverse micelles. It was found that the energy transfer efficiency in homogeneous solutions was improved in micelles and reverse micelles due to an increased encounter probability. In fact it was further established that reverse micelles provided a better medium for energy transfer in this case as was reflected from

the energy transfer parameters¹⁰. Within the reverse micelles, smaller water pool facilitates energy transfer due to better proximity between the donor and acceptor¹⁰. It has also been revealed that due to the less steric bulk, acridine orange performed better in FRET than the fluorescein. Since these dye molecules are all biologically significant, FRET provides valuable insight into the application of energy transfer studies to determine distances in biological systems using external fluorescent labels.

In protein environment

Given the broad range of biological activities of the probe AODIQ, and to assess the probable location of the probe in the protein environment we have been interested in the FRET studies between HSA/BSA and AODIQ¹¹. The tryptophan moiety present in the serum albumins absorbs appreciably at 280 nm giving a broad fluorescence with maximum at around 340-350 nm. The molecule AODIQ does not absorb significantly at 280 nm but absorbs appreciably at 350 nm. The fluorescence of AODIQ in HSA environment comes out with a maximum at 488 nm. Considering the fluorescence band of tryptophan and the absorption band of AODIQ, the pair was judged as a promising pair of donor-acceptor systems for the FRET study (Fig. 7).

On gradual addition of AODIQ, fluorescence intensity of the tryptophan residue present in HSA decreased with a concomitant increase in the fluorescence intensity of AODIQ through an isoemissive point at 438 nm (Fig. 8). This indicates an efficient energy transfer from the tryptophan residue present in HSA to AODIQ.

As stated earlier for other cases, we observed neither any additional absorption band for the mixture of HSA and AODIQ nor any deformity in the spectral pattern

of the HSA-AODIQ system from that of the resultant of the individual absorption spectra corresponding to the donor and the acceptor taking into consideration the composition of the components in the mixture. Furthermore, the fluorescence spectrum of the mixture of donor and acceptor did not show any additional new band other than the individual emission bands of the two components. These factors taken together negate the formation of any permanent ground-state complex between the donor-acceptor pair in the solution as well as the formation of exciplex between the excited donor and the unexcited acceptor molecules¹¹. Förster's distance (R_0) is calculated assuming random orientation of the donor and acceptor molecules. Thus, from equation (10), we have calculated R_0 to be 73.6 Å taking $\kappa^2 = 2/3$, $n = 1.333$ (water), $\phi_D = 0.14$.

The energy transfer efficiency (Φ) for the pair of HSA and AODIQ in case of 1:1 composition (10 μM each) has been

calculated to be 0.15, using equation (8). With a knowledge of the energy transfer efficiency (Φ) and the critical energy transfer distance (R_0), the distance (R) between the donor and the acceptor molecule has been calculated to be 98.3 Å using relation (9)⁵. Since in the present case the energy transfer efficiency is 0.15 (< 50%), one should expect a value of R greater than R_0 . Thus, the determined value of R is rationally acceptable.

Similar measurements have also been successfully performed in the case of FRET between peptide mellitin and dansyl, i.e. 5-dimethylamino-1-naphthalenesulfonic acid by Lakowicz et al¹². There has been a single dansyl acceptor adjacent to each tryptophan donor and the helical structures ensured a single donor-acceptor distance. Hence, the theory described above could be easily exploited to calculate the D-A distance also in this case. Another work by Patel and Dutta¹³ gives a FRET analysis of the fluorescence quenching of HSA by chlorin p_6 and purpurin 18 suggesting that the distance

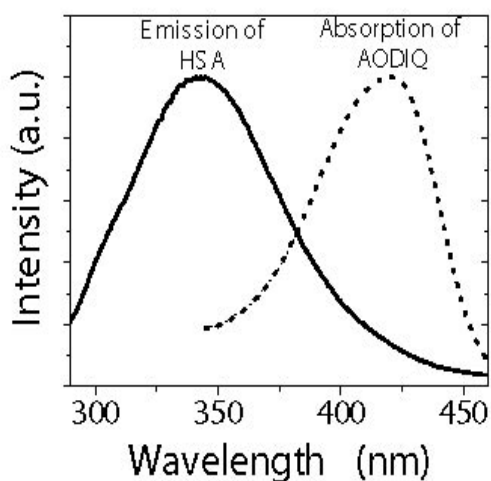


Fig. 7. Overlap of fluorescence spectrum of HSA (solid line) and absorption spectrum of AODIQ (dotted line).

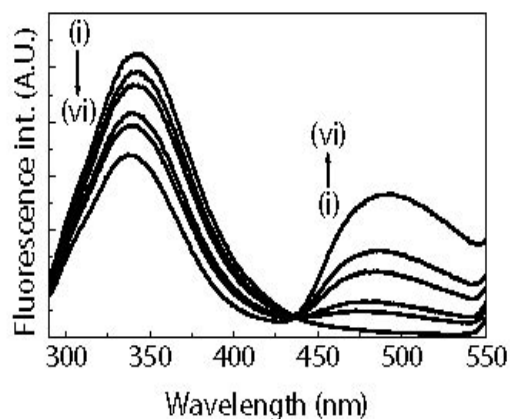


Fig. 8. Fluorescence spectra of HSA as a function of AODIQ concentrations ($\lambda_{exc} = 280 \text{ nm}$) in aqueous HEPES buffer solution. Curves (i) \rightarrow (vi) correspond to 0, 4.4, 6.5, 13.1, 17.4, 21.8 μM AODIQ concentrations. HSA concentration was 10 μM .

of the binding sites of the chlorins from the lone tryptophan residue is similar to that of the Sudlow's Site I, which is present in the domain II. Global analysis of the time-resolved data performed by the authors also reveals the displacement of warfarin from its conjugates with HSA by both the chlorines, thereby confirming the residence of these photosensitizers in the warfarin-binding Sudlow's Site I.

In liposome environment

FRET studies have also been performed in membrane environments, *viz.*, lipid bilayers etc. A couple of citations in this context are provided in this segment to justify the broad applicability of FRET as a 'spectroscopic ruler'.

In a study by Li et al, the dansyl fluorophore was used as a donor and polydiacetylene (PDA) as acceptor to demonstrate the modulation of FRET through conformationally induced changes in the PDA absorption spectrum following thermal treatment that significantly converts the PDA backbone of the liposome from blue to red form¹⁴. In course of the work it is proposed that more efficient energy transfer occurs between the dansyl to the red form of PDA liposome. The significance of the study lies in the fact that it provides a basis of a new sensing platform based on J-modulated FRET as an actuating mechanism.

Another study concerning FRET in liposome vesicles is that of Seth et al. This involves energy transfer using the substituted coumarin dyes as the donor and rhodamine 590 (Rh6G) as the acceptor, investigated in lecithin vesicles and sodium taurocholate (NaTC)-lecithin mixed aggregates using steady state and time resolved fluorescence spectroscopy¹⁵. Energy transfer parameters were calculated using the given equations. It was found that with addition of NaTC in

lecithin the rate of energy transfer in case of coumarin 153 was not affected significantly while that in the case of coumarin 151 decreases to half. This was rationalized in the light of the deeper location of coumarin 153 in the lipid bilayers or mixed aggregates. Thus the relative orientation of the FRET partners was proposed to play a significant role in the energy transfer process.

Conclusion

Fluorescence resonance energy transfer (FRET) or *resonance energy transfer* (RET) is a diverse and rapidly changing topic of research. It is therefore actually impossible to provide a complete illustration of this excellent photoprocess in a single essay. Our attempt has therefore been to cite a few examples of this photoreaction in different environments, to illustrate the wide applicability of FRET in determining distances between the two partners involved in the process. Emphasis has been given in this essay on works from our laboratory, though in an attempt to cover the wide spectrum of applicability of FRET, citations from other laboratories have also been made. Indeed these illustrations help to justify the name of FRET as a true 'spectroscopic ruler'.

Acknowledgements

Financial supports from DST, DBT and CSIR, Government of India, are gratefully acknowledged. D.S. and P.D. thank CSIR for the research fellowships.

References

1. Turro N.J., Modern Molecular spectroscopy, The Benjamin/Cummings Publishing Co., Inc (1978).
2. Lakowicz J.R., Principles of Fluorescence Spectroscopy, Plenum Press: New York (1999).
3. Förster T., Ann. Phys. 437, 55 (1948).
4. Jockusch S., Timpe H.J., Schnabel W. and Turro N. J., J. Phys. Chem. A. 101, 440 (1997).

5. Mallick A., Haldar B., and Chattopadhyay N., J. Phys. Chem. B. 109, 14683 (2005).
6. Mallick A., Haldar B., Sengupta S. and Chattopadhyay N., J. Lumin. 118, 165 (2006).
7. Das P., Mallick A., Purkayastha P., Haldar B. and Chattopadhyay N., J. Mol. Liq. 130, 48 (2007).
8. Kozyra K.A., Heldt J.R., Diehl H.A. and Heldt J., J. Photochem. Photobiol. A. 152, 199 (2002).
9. Mallick A., Haldar B., Maiti S. and Chattopadhyay N., J. Colloid. Interface Sci. 278, 215 (2004).
10. De S., Girigoswami A. and Mandal A.K., Spectrochimica Acta Part A. 59, 2487 (2003).
11. Das P., Mallick A., Haldar B., Chakrabarty A. and Chattopadhyay N., J. Chem Sci. 119, 77 (2007).
12. Lakowicz J.R., Gryczynski I., Wiczak W., Laczko G., Prendergast F. C. and Johnson M.L., Biophys. Chem. 36, 99 (1990).
13. Patel S. and Dutta A., J. Phys. Chem. B. 111, 10557 (2007).
14. Li X., McCarroll M. and Kohli P., Langmuir 22, 8615 (2006).
15. Seth D., Chakraborty A., Setua P., Chakrabarty D. and Sarkar N., J. Phys. Chem. B. 109, 12080 (2005).



Deboleena Sarkar graduated in Chemistry Honours from Presidency College, Calcutta under Calcutta University in the year 2005. She did her Masters from the same institute in 2007. At present she is pursuing research in photochemistry at Jadavpur University with a CSIR junior research fellowship.



Paramita Das graduated in Chemistry Honours from Jaipuria College, Calcutta under Calcutta University in the year 2002. She did her Masters from Calcutta University in 2004. She has been pursuing research in photochemistry at Jadavpur University since 2006. At present she is enjoying a CSIR senior research fellowship.



Dr. Nitin Chattopadhyay did his Graduation and Masters from Calcutta University. He worked with Prof. Mihir Chowdhury at I.A.C.S. (Calcutta, India) and obtained his PhD degree in 1990 from Jadavpur University (Calcutta, India). Currently he is Professor in the Department of Chemistry, Jadavpur University. During his postdoctoral assignments in different phases he worked with Profs. F. C. De Schryver and M. Van der Auweraer in Katholieke Universiteit Leuven, Belgium and with Profs. S.J. Formosinho, L. G. Arnaut, H. D. Burrows and R. Fausto in Coimbra University, Portugal. His research interests include laser-induced optoacoustic spectroscopy, photophysical and photochemical processes (ESPT, ICT, electron transfer, charge transfer and energy transfer) in homogeneous and in microheterogeneous environments, fluorescence-based sensing, etc.

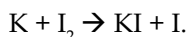
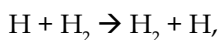
Experimental evidence of the involvement of triplet excited state in the photodissociation of hydrogen peroxide

Ranjan Das

Tata Institute of Fundamental Research
Homi Bhabha Road, Mumbai 400005, India

1. Introduction

The research on the molecular reaction dynamics aims to map a very detailed pathway of elementary chemical reactions. Here the chemical reaction from the reactants in a well-defined state is followed throughout the progress of the reaction to find out how the products are produced in well-defined states. In the words of Levine and Bernstein, in such studies "the intimate details of physical change and chemical reactivity can be observed experimentally and understood theoretically" [1]. Achievement of that goal requires, on the one hand, sophisticated experimental techniques and, on the other, highly accurate quantum mechanical methods for predicting or explaining the outcome of the experiment. The chemical systems which are studied in this way generally consist of few atoms, so that the number of degrees of energy distribution is kept small and the experiments can be devised to probe well-defined states. At the same time, as the number of atoms is few, high-quality quantum mechanical calculations are possible. Most of the studies therefore probe triatomic chemical reactions of the type $A + BC \rightarrow AB + C$. Some typical examples of such reactions are



Hydrogen peroxide, H_2O_2 , in this scenario is a typical tetra-atomic molecular

system whose photodissociation dynamics in the gas phase has been extensively studied by experimental and theoretical techniques [2-10]. On photoexcitation, H_2O_2 dissociates into a pair hydroxyl radicals. A consequence of this is that the electronic absorption spectrum of H_2O_2 has no absorption band, but shows a featureless continuum of absorption starting around 300 nm and monotonically rising at shorter wavelengths [6]. The dissociation of H_2O_2 in the gas phase is estimated to take place in less than 60 fs after photoexcitation [1], and the quantum yield of the OH radical is found to be 2 [4]. Detailed internal state distribution (vibration, rotation, spin and Λ components), translational energy distribution and anisotropy, angular distribution, rotational alignment, and vector correlation between rotational and translational motion of the product OH radicals have been measured [3, 5]. It has been established that the OH radicals so produced are vibrationally cold, while their rotational temperature is very hot at about 1500 K [3].

All the experimental results have been obtained by monitoring the photogenerated OH radicals, since the excited state of H_2O_2 is too short to be detected even by the most modern ultrafast spectrometers. As the ground state of H_2O_2 is a singlet, and the direct photoexcitation to a triplet state is forbidden, the dissociative state of H_2O_2 is believed to be a singlet state as well. All the experimental results have

been interpreted with the assumption that the dissociation is confined to the singlet excited state potential energy surface. The theoretical works, based on classical trajectory calculations on *ab initio* potential energy surfaces, also confine the dynamics of photodissociation of H_2O_2 to the singlet excited state and interpret the results [6-10].

There are two important reasons to examine the role of excited triplet states on the photodissociation of H_2O_2 . The first is theoretical: Semiempirical quantum mechanical calculations of Evleth [11, 12] show that there are 3 singlet excited states and 4 triplet excited states of H_2O_2 that correlate with the two hydroxyl radicals in their ground state as a function of the O-O bond distance of H_2O_2 . All these excited states are repulsive. Unless the intersystem crossing (ISC) probability from the singlet manifold to the triplet manifold of excited H_2O_2 is precisely zero, the triplet states should play a role in the photodissociation dynamics of H_2O_2 . The second reason is in the interpretation of experimental data: An important observation of the photodissociation of H_2O_2 , viz., the Λ -type preference of the OH radicals, in which the A'' component becomes increasingly dominant with increasing rotational angular momentum J [3], could not be satisfactorily explained by assuming that the dynamics of the photodissociation is restricted solely to the singlet excited potential energy surfaces of H_2O_2 . In order to account for the Λ -type preference of the OH radicals, Morita and Kato [13] assumed that dissociation of H_2O_2 involved the triplet potential energy surface. In justification of this assumption they theoretically calculated [13] the ISC transition probability of H_2O_2 from a singlet excited state to a triplet state resulting from spin-orbit interactions, incorporated in the

form of a Breit-Pauli Hamiltonian. These calculations show that the ISC transition probability increases rapidly as the O-O bond distance of H_2O_2 increases during the dissociation. Whereas this ISC probability is calculated to be only about 0.0016 at the equilibrium geometry of H_2O_2 , this value increases substantially to 0.44 as the O-O bond distance increases to 3 Å. Based on such a large probability of ISC during the stretching of the O-O bond of H_2O_2 , they were able to explain the Λ -type preference of the OH radicals during photodissociation.

If the photoexcited H_2O_2 is indeed undergoing the intersystem crossing from a singlet excited state to a triplet excited state, it would be a unique example of extremely fast intersystem crossing taking place during a single vibration of the O-O bond, as both the singlet and the triplet excited states are repulsive. It would thus be extremely important to obtain further experimental evidence in support of this phenomenon. We have attempted to obtain information on the nature of the photodissociative state of H_2O_2 from the electron spin polarisation studies on H_2O_2 in 2-propanol solvent using time-resolved electron paramagnetic resonance (TR-EPR) experiments. Our results strongly indicate that the dissociative state of H_2O_2 is a triplet state [14]. The present article is an expository one based on that finding.

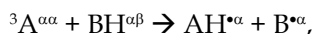
2. Electron spin polarisation and TR-EPR spectroscopy [15]

Transient free radicals which are generated by a laser light pulse or a radiolysis pulse often show that the distribution of electron spins in different Zeeman-split levels deviates strongly from the Boltzmann distribution. As the intensity of the EPR spectrum of a paramagnetic species depends, among other things, on the difference in the spin population between

two levels connected by the EPR transition, the deviation of the spin distribution from the Boltzmann distribution is experimentally seen as anomalous line intensities of the EPR spectra. A fast-response time-resolved EPR spectrometer records such EPR spectra at a time that is shorter than the electronic spin-lattice relaxation time of the radical. Such EPR spectra reflect the non-Boltzmann spin distribution in the form of anomalous line intensities compared to spectra arising from the radical that has reached Boltzmann spin distribution.

The mechanisms through which radicals can acquire non-Boltzmann electron spin distribution can be understood by referring to Fig. 1, which shows typical photophysical and photochemical pathways of a molecule. Let us say a molecule A initially in the ground singlet state $|S_0\rangle$ is excited to an excited singlet state $|S_1\rangle$. Intersystem crossing, governed by the spin-orbit interaction, can bring the molecule to a triplet state. However, as the intersystem crossing is usually not isotropic for most molecules, the probability of the ISC from $|S_1\rangle$ to the three triplet sub-levels are not same. As a result, the three triplet sublevels, $|T_{+1}\rangle$, $|T_0\rangle$, and $|T_{-1}\rangle$ designated by the component of the spin angular momentum in the magnetic field of the EPR spectrometer, are unequally populated by the ISC. Thus the initial spin distribution in the three triplet sub-levels will be non-Boltzmann. Let us assume, for simplicity, that the $|T_{+1}\rangle$ state, with an α electron spin wavefunction, is predominantly populated. The spin-lattice relaxation processes in the triplet sublevels will try to restore the Boltzmann distribution. However, if the chemical reaction of the triplet molecule with a substrate competes with the electronic spin-lattice relaxation, the spin polarization of the triplet will be transferred to the

resultant radicals. As the $|T_{+1}\rangle$ state of A is assumed to be predominantly populated by the ISC, and the chemical reaction rate, k_{RXN} , with a substrate BH competes with the spin-lattice relaxation of the triplet, the chemical reaction would be given by



where the chemical reaction involves, for example, a hydrogen atom abstraction. The conservation of electron spin during the chemical reaction leaves both the radicals AH^\bullet and B^\bullet with the α electron spin. The TR-EPR spectrum of this system, recorded before the spin-lattice relaxation of the radicals can restore the thermal equilibrium with the surrounding, will show emissive EPR lines, as both the radicals are created with an α electron spin. This spin polarization will be *independent* of the hyperfine lines of the radicals. This mechanism is called the **triplet mechanism** (TM). In effect, TM predicts totally emissive or enhanced absorptive EPR signal intensities for both the radicals.

Whereas TM requires that the chemical reaction takes place in the excited triplet state with a rate that is comparable to, or faster than, the spin-lattice relaxation rate of the

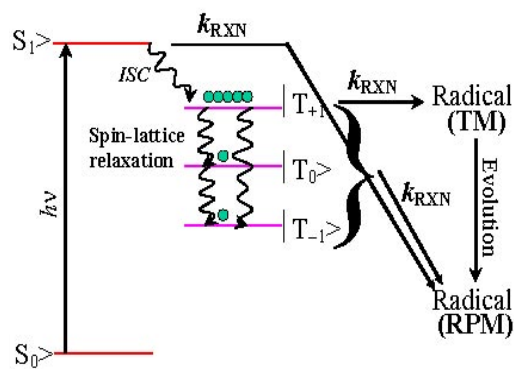


Fig. 1. Typical photophysical and photochemical processes leading to the formation of spin polarised free radicals. The non-Boltzmann populations in the triplet sub-levels are indicated by the number of small balls.

triplet, there is another mechanism, called the **radical pair mechanism (RPM)**. RPM produces electron spin polarised radicals when the reaction takes place either in the singlet or the triplet excited state, and in the latter case, the rate of the reaction is unable to compete with the triplet spin-lattice relaxation rate. For a triplet precursor, the three triplet sublevels first reach thermally equilibrated Boltzmann distribution and then all the three sublevels react with the substrate. Whether the singlet excited state or the thermally equilibrated triplet state reacts with the substrate, there is no electron spin polarisation at the time of generation of the pair of nascent radicals. This nascent radical pair undergoes diffusive motion in the solvent. They can move away from each other, and again come back and meet. During this process, if there is a small but finite difference in the precessional frequencies of the two radicals, a radical pair that is created in an overall singlet $|S\rangle$ spin pair from a singlet precursor can

evolve into an overall triplet $|T_0\rangle$ spin pair. Similarly, a radical pair that is created in an overall triplet $|T_0\rangle$ spin pair from a triplet precursor can evolve into a singlet $|S\rangle$ spin pair. Such an $|S\rangle$ - $|T_0\rangle$ mixing can take place as long as the radicals survive in the solution. The singlet radical pair may react to produce a diamagnetic product and disappear, whereas the triplet radical pair goes back to the solution without reacting, leaving the spins of the separated radicals polarised. The difference in the precessional frequencies of the radicals can arise either from their differences in the g -values, or the electron-nuclear hyperfine interactions. Very often the g -values of most of the organic free radicals differ little from one another, and it is the difference in the hyperfine interactions that controls the $|S\rangle$ - $|T_0\rangle$ mixing. This produces electron spin polarisation in the radicals that become *dependent* on the hyperfine lines, such that one half of the TR-EPR spectrum appears in emission (E) and the other half in absorption (A). For a

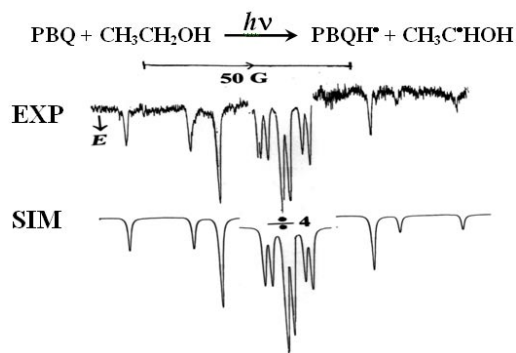


Fig. 2. Experimental (EXP) and simulated (SIM) TR-EPR spectra of *p*-benzoquinone-ethanol system, recorded at 0.5 μs after a 248 nm laser flash, at room temperature. The central triplet of doublets, shown in reduced gain, is due to the PBQH^\bullet radical, and the other lines are due to the $\text{CH}_3\text{C}^\bullet\text{HOH}$ radical. Predominantly emissive EPR lines of both radicals indicate that the triplet mechanism is the dominant spin polarisation mechanism. Adapted from [16] (© VSP 2005).

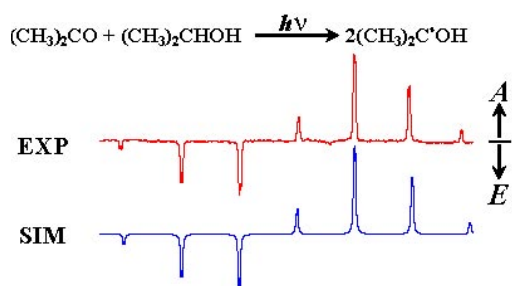


Fig. 3. Experimental (EXP) and simulated (SIM) TR-EPR spectra of acetone-2-propanol system, recorded at 0.5 μs after a 248 nm laser flash, at room temperature. The spectrum is due to the single radical $(\text{CH}_3)_2\text{C}^\bullet\text{OH}$. In this and the following figures, EPR signal going upwards is absorptive (A), and downwards is emissive (E), and the magnetic field increases from left to right. Predominantly E/A polarised EPR lines indicate that the radical pair mechanism from a triplet precursor is the dominant spin polarisation mechanism in this system.

singlet precursor, the overall pattern of the EPR spectrum is *A/E* (low field hyperfine lines are in absorption, and the high field hyperfine lines are in emission). For a triplet precursor, the pattern is *E/A* (low field hyperfine lines are in emission, and the high field hyperfine lines are in absorption). It must be mentioned that a radical pair created through the TM can also undergo $|S\rangle - |T_0\rangle$ mixing and produce further spin polarization due to the RPM during its subsequent time evolution.

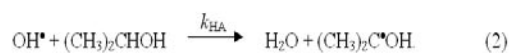
The two spin polarisation mechanisms, as described above, pertain to a geminate radical pair, which is created as a nascent pair whose initial spin state is the same as that of the precursor molecule producing the radicals. However, during the course of the evolution of the radicals, two radicals created independently can meet each other and undergo the $|S\rangle - |T_0\rangle$ mixing. Such radical pairs, called the random pairs, will also contribute to the electron spin polarisation according to the RPM. When a radical survives long enough to meet another independently generated radical, this random radical pair behaves as if they were generated from a triplet precursor molecule, irrespective of the true electronic state of the precursor. Thus, one has to apply caution in inferring the nature of the precursor solely from the polarisation pattern of the RPM polarized TR-EPR spectra. Such polarized radicals due to the random pair are seen predominantly in the free radicals produced in pulse radiolysis experiments. In laser flash photolysis experiments their contribution is generally seen at a later time after the geminate radical pair polarisation.

Figures 2 and 3, respectively, show examples of TM dominated and RPM dominated spin polarised TR-EPR spectra. In Fig. 2, the observation of essentially

emissive EPR spectra of both the radicals conclusively shows that the precursor is a triplet state, and the rate of the chemical reaction is comparable to the spin-lattice relaxation rate of the triplet state [16]. In Fig. 3, the observation of an *E/A* polarized EPR spectrum, as early as 0.5 μ s after the laser pulse, shows that the geminate radical pair is seen whose precursor is a triplet state.

3. Photodissociation of H_2O_2 and TR-EPR: the strategy

Our experimental strategy to establish the nature of the excited state of dissociating H_2O_2 was the following: We studied the photodissociation of H_2O_2 in 2-propanol *solution*. We make the reasonable assumption that the solvent does not influence the intersystem crossing process of the photoexcited H_2O_2 in 2-propanol. The ISC, governed by the spin-orbit interactions in H_2O_2 , would be an intramolecular process, and it will not be influenced by the solvent as 2-propanol does not have any heavy atom. The geminate pair of OH radicals will conserve the spin state of the precursor H_2O_2 . The OH radical is extremely reactive, and is known to abstract a hydrogen atom from solvents such as 2-propanol to give H_2O and a solvent radical. The reactions in 2-propanol are:



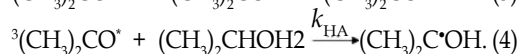
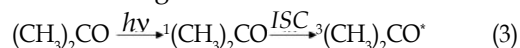
If reaction 2 is faster than the electronic spin-lattice relaxation of the OH radical, the spin state of the acetone ketyl radical, $(CH_3)_2C^{\bullet}OH$, would be the same as that of the OH radical. Thus if spin-polarised EPR spectra of $(CH_3)_2C^{\bullet}OH$ radical is seen in TR-EPR experiments on H_2O_2 -2-propanol system, we should be able to establish

the nature of the dissociative state of photoexcited H_2O_2 .

As noted above, in order for the above strategy to work, the rate of the hydrogen abstraction from 2-propanol by the OH radical must be able to compete with the electronic spin-lattice relaxation rate of the OH radical. There is no experimental value of this spin-lattice relaxation rate. But this rate is known to be very fast. The inability to observe the EPR spectrum of the OH radical in liquids is attributed to its very broad EPR linewidth due to its extremely fast electron spin relaxation [17]. The inefficient quenching of the electronic orbital angular momentum of the OH radical is believed to be the origin of such fast spin relaxation. Based on the modulation of the spin-orbit coupling caused by the formation and breaking of hydrogen bonds of the solvent molecule with the OH radical, Brocklehurst [18] has estimated the spin-lattice relaxation time of the OH radical to be approximately 0.5 ns in water at room temperature. In their pulse radiolysis experiments, Verma and Fessenden [19] have also estimated this relaxation time be less than 1 ns at room temperature, when they could not see any initial spin-polarisation on the secondary radicals generated by the OH radical. Recently, Fessenden has revised this estimated value to about 100 ps [20]. As the temperature is lowered, this value is likely to increase, because the correlation time increases with the viscosity of the solution. The rate constant of the hydrogen abstraction reaction by the OH radical with 2-propanol in aqueous solutions has been determined by various studies and their values tabulated [21]. The value at room temperature is $\approx 2 \times 10^9 \text{ M}^{-1}\text{s}^{-1}$. This nearly diffusion-controlled rate constant indicates that in aqueous solution a hydroxyl radical has to diffuse to an alcohol molecule for

the reaction to occur. In our system, as the solvent itself is the donor of hydrogen atom, diffusion would not be the rate determining step, as the OH radical would find the solvent molecule in its immediate vicinity for reaction. Thus we could assume that the hydrogen abstraction rate constant in our system would be $\geq 2 \times 10^9 \text{ M}^{-1}\text{s}^{-1}$. This gives an effective pseudo-first order rate constant of $\geq 2.4 \times 10^{10} \text{ s}^{-1}$ in the 2-propanol solvent of concentration of about 12 M. Consequently, the effective lifetime of the OH radical in 2-propanol is expected to be ≤ 40 ps. This lifetime is clearly comparable to, and in fact shorter than, the estimated spin-lattice relaxation time of 100 ps. Thus the estimated values of the spin relaxation rate and the hydrogen abstraction rate of the OH radical are such that the hydrogen abstraction reaction could compete with the spin relaxation, so that the spin orientation of the nascent OH radical should be transferred to the $(\text{CH}_3)_2\text{C}^\bullet\text{OH}$ radical.

In our studies, we also compared the results of H_2O_2 in 2-propanol with those of the well-studied acetone–2-propanol system. Here a photoexcited acetone molecule in its triplet state abstracts a hydrogen atom from 2-propanol giving rise to a pair of $(\text{CH}_3)_2\text{C}^\bullet\text{OH}$ radicals [22–26], according to the following reactions



TR-EPR spectrum of this system has been used as an example of RPM polarisation in Fig. 3. These comparative studies will show the similarities in the spin dynamics of the two systems.

We used our home-built time-resolved EPR spectrometer coupled with an excimer laser (KrF fill, wave length: 248 nm, energy: 30 mJ/pulse at 30 Hz) to record the TR-EPR spectra [16] for our experiments.

4. Results and discussions

Fig. 4 shows the TR-EPR spectra recorded in H_2O_2 in 2-propanol and acetone in 2-propanol systems, at room temperature, and at various delay times after the laser flash. The seven-line spectrum with E/A polarisation is due to the $(\text{CH}_3)_2\text{C}\cdot\text{OH}$ radical. The nature of the EPR spectra and their time dependence are essentially same in both the systems. In the acetone-2-propanol system, the E/A polarised spectra originate dominantly from the RPM from a triplet precursor, with a small component of a net absorptive signal. In the H_2O_2 -2-propanol system, the observation of similar spin polarised EPR spectra indicates that the nascent pair of OH radicals, generated from the dissociation of a H_2O_2 molecule, produced a pair of $(\text{CH}_3)_2\text{C}\cdot\text{OH}$ radicals which subsequently underwent spin evolution to produce the observed spin polarisation. This E/A polarisation strongly indicates that the precursor should be a triplet. However, the precursor of the $(\text{CH}_3)_2\text{C}\cdot\text{OH}$ radical in this system is the OH radical. Thus the pair of OH radicals must be produced in a spin-correlated triplet state

from a triplet excited H_2O_2 . The very fast hydrogen abstraction reaction of the OH radicals transfers this spin correlation to the secondary radical pair $(\text{CH}_3)_2\text{C}\cdot\text{OH}$ before the spin-lattice relaxation of OH radical can destroy the spin correlation. Since the direct photoexcitation of H_2O_2 produces only an excited singlet state, the spin polarised EPR spectra show that during dissociation, H_2O_2 undergoes extremely efficient ISC to a triplet state which produces the pair of OH radical in a spin-correlated triplet state. The probability of the ISC of acetone from its singlet excited state to a triplet state is known to be nearly 1.0 at room temperature [27]. From the comparison of the intensities of the RPM signals of the $(\text{CH}_3)_2\text{C}\cdot\text{OH}$ radical in the H_2O_2 -2-propanol system and the acetone-2-propanol system, it appears that the probability of the excited singlet H_2O_2 undergoing ISC to its triplet states during dissociation should also be much higher than 0.5. This may be compared with the value of 0.44, which was calculated by Morita and Kato [13].

We have discussed earlier that in order to establish the nature of the precursor state most unequivocally from the nature of the RPM polarised EPR spectra, one must ensure that one is observing the polarisation due to the geminate radical pair and not due to the random radical pair. This applies to our H_2O_2 -2-propanol system as well. To give more convincing evidence on the nature of the dissociative state of H_2O_2 , we attempted to detect the presence of a spin-correlated radical pair state [28, 29] of $(\text{CH}_3)_2\text{C}\cdot\text{OH}$ radicals. Fig. 5 shows the time-resolved

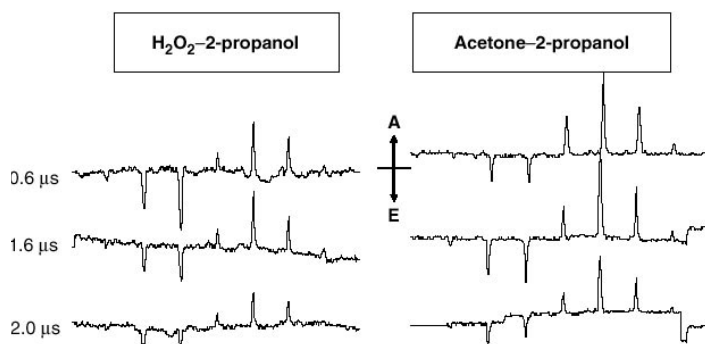


Fig. 4. Time-resolved EPR spectra of $(\text{CH}_3)_2\text{C}\cdot\text{OH}$ radical in H_2O_2 -2-propanol and acetone-2-propanol systems at 22 °C, recorded at different delay times after a 248-nm laser flash. Both the systems show very similar features and time dependence. In this and the following figure, $[\text{H}_2\text{O}_2] = 4\% \text{ v/v}$, $[\text{Acetone}] = 5\% \text{ v/v}$. Reproduced from [14] (© Taylor & Francis 2007)

EPR spectra recorded at $-32\text{ }^{\circ}\text{C}$, at various delay times after the laser flash. At such low temperature, the viscosity of the sample increases considerably and the two radicals of the radical pair are held in close proximity. This produces a characteristic "anti-phase" line [28, 29], particularly in the central hyperfine line of the $(\text{CH}_3)_2\text{C}\cdot\text{OH}$ radical. Such a feature is indicative of the spin-correlated $(\text{CH}_3)_2\text{C}\cdot\text{OH}$ radical pair generated from a triplet precursor in the acetone-2-propanol system, when extra transitions are possible due to the dipolar and/or exchange interactions between the two radicals of the pair held in close proximity. A similar feature in the H_2O_2 -2-propanol system confirms the presence of such spin-correlated radical pairs generated from a triplet precursor in this system as well. This, in turn, confirms that the dissociation

of H_2O_2 takes place predominantly from an excited triplet potential energy surface. This "anti-phase" characteristics disappeared in less than $3\text{ }\mu\text{s}$ after the laser flash. This decrease in the "anti-phase" signal with time, and its eventual disappearance, is attributed to the separation of the geminate radical pair created by the primary photochemical reaction after the laser pulse.

5. Conclusion

From the known estimates of the spin relaxation rate and the hydrogen abstraction rate of the OH radical, we showed that these two rates could be comparable. Then, from a comparative study of spin polarisation of the $(\text{CH}_3)_2\text{C}\cdot\text{OH}$ radical, generated photolytically in the H_2O_2 -2-propanol and acetone-2-propanol systems, we have shown that the dominant dissociative route of H_2O_2 involved the triplet excited state. As the photoexcitation of H_2O_2 produces an excited singlet state, these results indicate that during a single vibration of the O-O bond of H_2O_2 , extremely fast ISC transfers the excited molecule from the singlet potential energy surface to a triplet surface. Not only does this show a unique case of extremely fast intersystem crossing, the results also imply that a proper analysis of the dynamics of photodissociation of H_2O_2 should include the triplet excited states as well.

References:

- [1] R. D. Levine and R. B. Bernstein, *Molecular Reaction Dynamics and Chemical Reactivity*, Oxford University Press, New York, 1987.
- [2] S. Klee, K.-H. Gericke, and F. J. Comes, *J. Chem. Phys.* 85, 40 (1986).
- [3] K.-H. Gericke, S. Klee, F. J. Comes, and R. N. Dixon, *J. Chem. Phys.* 85, 4463 (1986).
- [4] G. L. Vaghjiani and A. R. Ravishankara, *J. Chem. Phys.* 92, 996 (1990).
- [5] M. P. Docker, A. Hodgson, and J. P. Simons, *Chem. Phys. Lett.* 128, 264 (1986).
- [6] R. Bershon and M. Shapiro, *J. Chem. Phys.* 85,

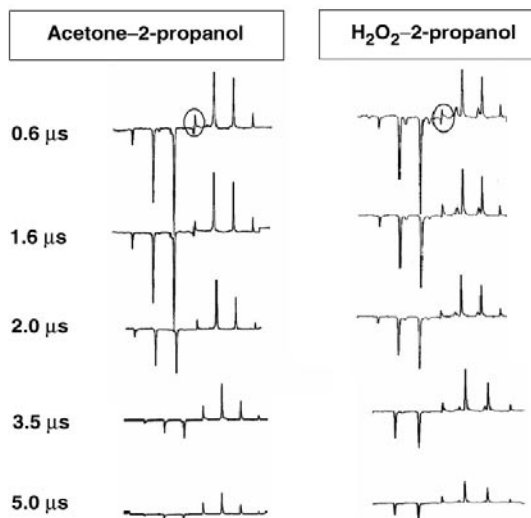


Fig. 5. Time-resolved EPR spectra of the $(\text{CH}_3)_2\text{C}\cdot\text{OH}$ radical in H_2O_2 -2-propanol and acetone-2-propanol systems at $-32\text{ }^{\circ}\text{C}$, recorded at different delay times after a 248-nm laser flash. The "anti-phase" or dispersive-type line shape of the central hyperfine line, observed at $0.6\text{ }\mu\text{s}$, has been encircled. Both the systems show very similar features and time dependence. Reproduced from [14] (© Taylor & Francis 2007)

- 1396 (1986).
- [7] R. Schinke and V. Staemmler, *Chem. Phys. Lett.* 145, 486 (1988).
- [8] R. Schinke, *J. Phys. Chem.* 92, 4015 (1988).
- [9] D. H. Zhang and J. Z. H. Zhang, *J. Chem. Phys.* 98, 6276 (1993).
- [10] Z. T. Cai, D. H. Zhang, and J. Z. H. Zhang, *J. Chem. Phys.* 100, 5631 (1994).
- [11] E. M. Evleth, *J. Am. Chem. Soc.* 98, 1637 (1976).
- [12] E. M. Evleth and E. Kassab, *J. Am. Chem. Soc.* 100, 7859 (1978).
- [13] A. Morita and S. Kato, *J. Phys. Chem.* 96, 1067 (1992).
- [14] B. Bhattacharjee and R. Das, *Molec. Phys.* 105, 1053 (2007).
- [15] L. T. Muus, P. W. Atkins, K. A. McLauchlan, and J. B. Pedersen, Eds. *Chemically Induced Magnetic Polarization* (Reidel, Dordrecht, 1977).
- [16] R. Das and B. Venkataraman, *Res. Chem. Intermed.* 31, 167 (2005).
- [17] M. C. R. Symons, *J. Am. Chem. Soc.* 91, 5924 (1969).
- [18] B. Brocklehurst, *J. Chem. Soc. Faraday Trans. II*, 75, 123 (1979).
- [19] N. C. Verma and R. W. Fessenden, *J. Chem. Phys.* 65, 2139 (1976).
- [20] R. W. Fessenden, private communication (2006).
- [21] L. M. Dorfman and D. E. Adams, *Reactivity of the Hydroxyl Radical in Aqueous Solution*, NSRDS-NBS 46 (National Bureau of Standards, Washington, 1972), p. 24.
- [22] S. K. Wong, T.-M. Chiu, and J. R. Bolton, *J. Phys. Chem.* 85, 12 (1981).
- [23] K. Y. Choo and J. K. S. Wan, *J. Am. Chem. Soc.* 97, 7127 (1975).
- [24] S. Yamauchi, K. Tominaga, and N. Hirota, *J. Phys. Chem.* 90, 2367 (1986).
- [25] S. Basu, A. I. Grant, and K. A. McLauchlan, *Chem. Phys. Lett.* 94, 517 (1983).
- [26] P. R. Levstein and H. van Willigen, *J. Chem. Phys.* 95, 900 (1991).
- [27] F. Wilkinson, in *Organic Molecular Photophysics*, edited by J. B. Birks (John Wiley, London, 1975) p. 95.
- [28] C. D. Buckley, D. A. Hunter, P. J. Hore, and K. A. McLauchlan, *Chem. Phys. Lett.* 135, 307 (1987).
- [29] G. L. Closs, M. D. E. Forbes, and J. R. Norris, *J. Phys. Chem.* 91, 3592 (1987).



Dr. Ranjan Das is an Associate Professor in the Department of Chemical Sciences at TIFR, Mumbai. His research interests are primary processes in photochemistry, spin polarisation and evolution of free radicals in photochemical reactions, and spin relaxation mechanisms in electron paramagnetic resonance spectroscopy.

**9th TROMBAY SYMPOSIUM ON RADIATION &
PHOTOCHEMISTRY (TSRP 2008) HELD AT YASHWANTRAO
CHAVAN ACADEMY OF DEVELOPMENT ADMINISTRATION
(YASHADA), PUNE: A REPORT**

Trombay Symposium on Radiation & Photochemistry (TSRP 2008) was held at Yashwantrao Chavan Academy of Development Administration (YASHADA), Pune, during January 7 – 11, 2008. This symposium organized by the Radiation & Photochemistry Division, BARC, was the 9th of the series of TSRP and was held in a venue outside Mumbai for the first time. The symposium was sponsored by the Board of Research in Nuclear Sciences (BRNS) in collaboration with Indian Society for Radiation & Photochemical Sciences (ISRAPS). The main objective of this symposium was to discuss the most recent developments in the field of radiation and photochemistry and their applications. About 250 scientists and students both from India and abroad participated in the symposium.

Dr. D. K. Palit, co-Convener of the symposium, welcomed the participants. Dr. T. Mukherjee, Director, Chemistry Group and the Chairman of the Symposium Organizing Committee, gave an introduction to the TSRP series of conferences held before and the present one. Dr. S. K. Sarkar, Head, Radiation & Photochemistry Division, BARC, elaborated the different important aspects of TSRP 2008. Dr. S. Banerjee, Director, BARC, inaugurated the symposium by lighting a lamp and released the proceedings of TSRP 2008 and the special issue of the ISRAPS Bulletin. In his inaugural address, he emphasized the role of radiation and photochemistry in the ongoing programme of DAE. The inauguration function concluded with a formal vote of thanks by Dr. T. Bandyopadhyay, co-Convener of the symposium.

The scientific program of the symposium included invited talks and contributed papers in the form of poster presentations. A total of fifty invited talks by speakers from India (16) as well as abroad (24) and 150 posters, including nine posters from abroad, were presented. The symposium covered the key areas of radiation & photochemistry, viz. (a) Ultrafast spectroscopy & dynamics of photoinduced chemical processes, (b) Gas phase reaction dynamics in bulk and beams, (c) Radiation & photochemistry in nuclear fuel cycle, (d) Radiation and photochemistry of atmosphere and environment, nanoscale materials as well as biological compounds, antioxidants and drugs, and (e) Industrial and societal applications of radiation and photochemistry. An exhibition of lasers, optics, detectors and other industrial products was arranged for two days in the symposium venue. Symposium Organizing Committee arranged a cultural programme on Indian Classical Dance & Music in unison with world music presented by Cosmic-Nad, Pune, in the evening of January 8. The programme was well-appreciated by the delegates of the symposium, particularly by the participants from abroad. Ten students below the age of 32 were awarded the 'Best Poster Presentation' awards by the Indian Society for Radiation & Photochemical Sciences (ISRAPS). Dr. Sharmistha Dutta Chowdhury of Radiation & Photochemistry Division, BARC, was awarded the 'P. K. Bhattacharyya Memorial Award' given by ISRAPS.

In the concluding session, Dr. Jai Pal Mittal, the Raja Ramanna Fellow of BRNS and the past President of ISRAPS, presented a brief summary of the symposium and expressed

satisfaction over the gradual improvement in the quality of the TSRP series of symposium following its inception in the year of 1992. This was followed by the feedback comments from the invited speakers from abroad as well as young student participants, who appreciated the excellent arrangements as well as the extremely high standard of the scientific contents of the talks and the posters presented in the symposium.



*Call for Nominations***Dr. P. K. Bhattacharyya Memorial Award**

Indian Society for Radiation and Photochemical Sciences (ISRAPS) has instituted the 'Dr. P.K. Bhattacharyya Memorial Award' to be awarded annually to a young Indian scientist, who has made outstanding contributions in the field of radiation and photochemistry.

Dr. Pijush Kanti Bhattacharyya (1935 - 2002), the 'Founder Secretary' of the Indian Society for Radiation And Photochemical Sciences (ISRAPS) during 1984 -1992, was a major force behind its formation. ISRAPS is an organization devoted to promote education, advancement and applications of radiation and photochemical sciences in India. He was one of those few scientists, who initiated research in the field of radiation- and photo-chemistry in India. He contributed significantly to the study of radiation effects on materials used in the reprocessing of spent nuclear fuel, radiation processing of materials, radiation induced colouring of diamonds and radiation- and photo-chemical investigations on many organic and inorganic molecules.

The award carries an amount of Rs. 1000/- in cash, a citation and a bronze medal, which will be presented to an awardee every year during either the Trombay Symposium on Radiation and Photochemistry (TSRP) or National Symposium on Radiation and Photochemistry (NSRP).

Eligibility

Citizens of Indian nationality below 32 years of age as on December 31, 2008 and working at least for five years to make significant contributions in the field of photo and radiation chemistry are eligible to be nominated. It may be noted that the award would be given for the research work carried out only in India.

Nominations

Name of the candidate may be proposed by a member of the Executive Council of ISRAPS, Head of the Institution to which the candidate belongs or a Bhatnagar Prize winner in the field of radiation and photochemistry. The nomination should be as per the proforma given below. The nomination, complete in all respects should reach the Hon. Secretary, ISRAPS, on or before Nov. 30, 2008.

Selection

An expert panel will scrutinize the applications for the award. The awardee has to present her / his work during NSRP-2009 which will be held at Kumaun University, Nainital during March 12-14, 2009. The awardee will be provided with DA and to-and-fro train-fare by AC-3-tier, if the awardee can not get the same from any other source. It may please be noted that the decision of the expert panel is final and canvassing in any form is a disqualification.

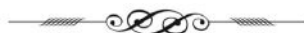
Completed application may please be forwarded to

Dr. Tapan K. Ghanty, Hon. Secretary, ISRAPS.

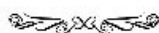
C/o Theoretical Chemistry Section, Chemistry Group, BARC, Mumbai 400 085.

Proforma for Application

1. Name of the nominee in full
2. Date and place of Birth (Enclose certificate of age duly attested)
3. Address (With Telephone and e-mail)
(a) Office (b) Residence
4. Academic Qualifications (in tabular form)
5. Details of Employment
6. Awards / Recognitions
7. List of publications
8. A summary (not exceeding 500 words) highlighting the significant research contribution.

**ISRAPS MEMBERS HONOURED**

Dr. A. K. Tyagi, presently Head, Solid State Chemistry Section, Chemistry Division, BARC and member ISRAPS was conferred with Homi Bhabha Science & Technology Award-2006, which is the highest award in DAE, on 11th May, 2008 by Dr. A. P. J. Abdul Kalam, former President of India In recognition of his seminal contributions in the field of nuclear materials, nanomaterials and functional materials.



Dr. Ravi Joshi of Radiation & Photochemistry Division, Chemistry Group, Bhabha Atomic Research Centre was awarded Young Scientist Award by Department of Atomic Energy, for the year 2006, for his notable contributions in the areas of free radical induced redox reactions using electron pulse radiolysis technique; kinetics and mechanism of reactions of free radicals with biomolecules, natural products and drugs; solvent effects on the chemical reactions and structure of transient species.

OBITUARY**Dr. Hari Mohan
(15.11.1944 to 13.02.2008)**

Dr. Hari Mohan, a well known radiation chemist, passed away in Mumbai on 13th February, 2008, at the age of 64. He is survived by his wife, Vinita two sons and one grandson. Born on 15th November, 1944 in Ludhiana, Punjab in a business community, Hari Mohan completed B. Sc. degree in Chemistry from Punjab University, Chandigarh in 1965. Immediately after graduation he joined the 10th batch of BARC training school and subsequently became Scientific Officer in the Radiation Chemistry Section of Chemistry Division, BARC. He continued his research career in the same field till his retirement in 2004 as the Head of the Section. During his service in BARC, he completed his Master's degree in 1972 and Doctoral degree in 1981 from Mumbai University. He was a post-doctoral fellow at the Hahn-Meitner Institute, Berlin (presently rechristened as Helmholtz Centre, Berlin), Germany from 1986 to 1987 and a visiting scientist at the University of Leipzig, Germany, in 1997.

Dr. Hari Mohan did pioneering work in the fields of radiation induced polymerization, radiation chemistry of halogen and sulfur compounds, pulse radiolysis studies of radical cations and published nearly 220 papers in peer reviewed national and international journals. A total of five doctoral theses were completed under his supervision. He was invited in many national and international conferences.

Dr. Hari Mohan was instrumental in the development of BARC-Pune University collaborative programme and more than ten doctoral students from Pune University were benefited from his guidance.

Dr. Hari Mohan was elected as a Fellow of the Maharashtra Academy of Sciences in 1998 and National Academy of Sciences, India in 1999. He was recipient of BARCOA award for nuclear sciences in 1993.

Even after superannuating, Dr. Hari Mohan continued his research interest in radiation chemistry and was a regular visiting scientist at National Center for Free Radical Research (NCFRR), Pune, and was active even the day before his death. He has been a good friend, advisor and mentor for many young radiation chemists. He was one of the active members of the Indian Society for Radiation and Photochemical Sciences, (ISRAPS) right from its inception and served in various capacities such as Executive Council Member and Treasurer.

With his passing away the Radiation Chemistry Community has lost a highly respected member, a kind mentor, a true gentleman and a very good friend.

ISRAPS deeply mourns the sudden demise of Dr. Hari Mohan.

Contents

Editorial	1
Message from the President and Secretary	3
Tracking dynamic events in biology using fluorescence: From macromolecules in test tube to cells deep inside living animals (R. Swaminathan)	5
Application of reorganization energy calculation in the determination of critical micellar concentration of a micelle (Priyanka Bolel and Mintu Halder)	8
Synthesis and spectroscopy of photoluminescent CdS and CdS:Mn²⁺ nanoparticles (Debabrata Mandal)	15
Fluorescence studies on photoinduced intramolecular processes in homogeneous and biomimetic environments (Sivaprasad Mitra)	23
Fluorescence resonance energy transfer: A spectroscopic ruler (Deboleena Sarkar, Paramita Das and Nitin Chattopadhyay)	31
Experimental evidence of the involvement of triplet excited state in the photodissociation of hydrogen peroxide (Ranjan Das)	42
TSRP-2008 Report	51
Dr. P.K. Bhattacharyya Memorial Award	53
ISRAPS Members Honoured	54
Obituary	55

Published by ISRAPS, C/o RPCD, BARC, Mumbai 400 085